PHYSICAL REVIEW B **80**, 125121 (2009)

Long-range Coulomb interactions and nanoscale electronic inhomogeneities in correlated oxides

Vijay B. Shenoy,[1,*] Tribikram Gupta,[1,†] H. R. Krishnamurthy,[1,2,‡] and T. V. Ramakrishnan[3,1,2,§]
[1]*Centre For Condensed Matter Theory, Indian Institute of Science, Bangalore 560 012, India*
[2]*Jawaharlal Nehru Centre for Advanced Scientific Research, Jakkur, Bangalore 560 064, India*
[3]*Department of Physics, Banaras Hindu University, Varanasi 221 005, Uttar Pradesh, India*
(Received 12 April 2009; published 23 September 2009; corrected 28 September 2009)

Electronic, magnetic, or structural inhomogeneities ranging in size from nanoscopic to mesoscopic scales seem endemic and are possibly generic to colossal magnetoresistance manganites and other transition metal oxides. They are hence of great current interest and understanding them is of fundamental importance. We show here that an extension, to include long-range Coulomb interactions, of a quantum two-fluid ℓ-b model proposed recently for manganites [Phys. Rev. Lett. **92**, 157203 (2004)] leads to an excellent description of such inhomogeneities. In the ℓ-b model two very different kinds of electronic states, one localized and polaronic (ℓ) and the other extended or broad band (b) coexist. For model parameters appropriate to manganites and even within a simple dynamical mean-field theory (DMFT) framework, it describes many of the unusual phenomena seen in manganites, including colossal magnetoresistance (CMR), qualitatively and quantitatively. However, in the absence of long-ranged Coulomb interaction, a system described by such a model would actually phase separate, into macroscopic regions of l and b electrons, respectively. As we show in this paper, in the presence of Coulomb interactions, the *macroscopic* phase separation gets suppressed and instead nanometer scale regions of polarons interspersed with band electron puddles appear, constituting a kind of quantum Coulomb glass. We characterize the size scales and distribution of the inhomogeneity using computer simulations. For realistic values of the long-range Coulomb interaction parameter V_0, our results for the thresholds for occupancy of the b states are in agreement with, and hence support, the earlier approach mentioned above based on a configuration averaged DMFT treatment which neglects V_0; but the present work has features that cannot be addressed in the DMFT framework. Our work points to an interplay of strong correlations, long-range Coulomb interaction, and dopant ion disorder, all inevitably present in transition metal oxides as the origin of nanoscale inhomogeneities rather than disorder frustrated phase competition as is generally believed. As regards manganites, it argues against explanations for CMR based on disorder frustrated phase separation and for an intrinsic origin of CMR. Based on this, we argue that the observed micrometer (meso) scale inhomogeneities owe their existence to extrinsic causes, e.g., strain due to cracks and defects. We suggest possible experiments to validate our speculation.

DOI: 10.1103/PhysRevB.80.125121 PACS number(s): 75.47.Lx, 71.30.+h, 71.38.−k, 75.47.Gk

I. INTRODUCTION

In the last decade or so, a number of experiments on several families of transition-metal oxides have provided evidence[1,2] that these often consist of patches of two different kinds of electronic/structural/magnetic states. The patches range in size from nanometers to micrometers and can be static or dynamic. In doped manganites ($Re_{(1-x)}Ak_xMnO_3$, with Re and Ak being rare-earth and alkaline-earth ions, respectively) where this phenomenon seems most widespread, one can have insulating locally lattice distorted (in some cases charge ordered) regions coexisting with metallic lattice undistorted ones.[3–11] In cuprates, an antiferromagnetic (AF) insulating state and a metallic (or superconducting) state seem close in energy and may coexist under some conditions, e.g., as nanoscale stripes (see, for example, the references in Ref. 12). There is a view that the proximity of two states with very different long-range orders (LRO) is a defining characteristic of these systems. For example, such a view has been most forcefully put forth in the work of Dagotto and co-workers[9,13–15] on the basis of numerical simulations of finite-sized samples of simplified lattice models capturing one or more key features of manganites. In Ref. 15, models with Mn e_g electrons having Jahn-Teller coupling to classical phonons and double exchange coupling to Mn t_{2g} core spins and antiferromagnetic interactions J_{AF} between the core spins are studied for $x=0.25$ on lattices of size up to 12×12. The clean system has a first-order transition [ending at a bicritical temperature from a ferromagnetic metallic (F-M) phase for small J_{AF} to an antiferromagnetic (AF-I) charge ordered, insulating phase when J_{AF} crosses a threshold J_{AF-t}]. The magnetoresistance exhibits colossal magnetoresistance (CMR)-like features when J_{AF} is tuned to be in the vicinity of the transition coupling J_{AF-t}. But the tuning becomes less of a requirement in the presence of disorder, which further generates nanoscopic interpenetrating patches of the two regions. These are then argued to be generic features responsible for (nanoscale) two "phase" coexistence, colossal magnetoresistance (CMR) and other phenomena observed in manganites. Larger length scale (micronscale) coexistence is also attributed to disorder effects amplified by proximity to a critical value of competing parameters.[13] However, the existence of manganites with negligible frozen disorder but showing CMR and other characteristic phenomena[16] suggests that these effects are intrinsic and that nanoscale and micronscale inhomogeneities could arise from other intrinsic causes.

 ©2009 The American Physical Society

In particular, the Coulomb interaction which is inevitably present can play a significant role if the two phases involved have different charge densities and will suppress phase separation, leading to nanoscopic electronic inhomogeneity or phase coexistence. This is the ubiquitous effect that we investigate here quantitatively in conjunction with the two fluid ℓ-b model[17–19] proposed recently for manganites. This model invokes two very different types of electronic degrees of freedom, one polaronic and localized (called ℓ) with associated Jahn-Teller lattice distortion and the other (called b) forming a broad band, with no lattice distortion and moving around primarily on sites not occupied by the polarons. It has been shown[18,19] that this approach explains much of the unusual behavior of manganites qualitatively and quantitatively. The work here shows in detail how the inclusion of electrostatic Coulomb interactions in the ℓ-b model leads to nanometer scale inhomogeneities and quantifies this effect. More generally, our results describe the intrinsic emergence of such nanoscale electronic inhomogeneities in any many electron system with two very different microscopic states of comparable energy. The model is different from disorder based phase separation or domain formation as seen in computer simulations of simple models[9] or in statistical Imry-Ma-type[13,20] arguments. The frequently observed micron scale inhomogeneity in many manganites[3,6,7] is probably related to strain effects, which are long ranged and unscreened. There are no calculations of this effect although simulations of elastic strain effects and inhomogeneities in Jahn-Teller distorted lattice systems have been made[21] on simplified models.

Specifically, in the ℓ-b model, at each lattice site there can be two types of electrons, namely, a nearly localized polaronic one (called ℓ) with site energy $-E_{JT}$ and a broad band one [called b, with site energy zero (0) and hopping amplitude t]. There is a strong local repulsion U (we consider $U \to \infty$ in this work) present between the ℓ polaron and the b electron. The physical origin and parameters of this model for manganites are mentioned below (Sec. II A) and have been described in Refs. 17–19 and 22. If long-range Coulomb interactions are neglected, the system described by the model phase separates, i.e., the ground state consists of two separate phases, one a macroscopic region entirely of ℓ polarons at every site and the other consisting of occupied b band states, the b density being fixed by the requirement of uniformity of the chemical potential μ, whence μ must equal $-E_{JT}$. However, the two phases have very different charge densities. With respect to $ReMnO_3$, which has one e_g electron per site, as the reference state, the polaronic phase is neutral, while the b phase has a positive charge density of $1-\bar{n}_b$ per site. Furthermore, the doped alkaline-earth ions (most likely randomly distributed on the lattice) supply unit negative charge at each alkaline-earth site. The relevant "extended ℓb model" which includes long-range Coulomb interaction involving these charges is described in Sec. II B. It leads to the suppression of macroscopic phase separation and the formation of nanoscopic "puddles" of b electrons surrounded by regions with only ℓ polarons. We first present a simple analytical estimate of the size of these regions, in particular their dependence on V_0, the energy parameter that determines the strength of the long-range Coulomb interaction (Sec. II C). Next, we describe simulations that we have carried out on finite systems of size up to $20\times20\times20$, with the energy levels of the b electron puddles calculated quantum mechanically, and the Coulomb effects treated in the Hartree approximation. The method for the ground state determination is detailed in Sec. II D. The results of the simulations are described and discussed in Sec. III. The ℓ polarons are shown to form a Coulomb glass.[23] Electronic states in the b electron regions are occupied (up to the chemical potential μ) for a critical hole concentration $x > x_{c1}$; these puddles connect percolatively and the system is a metal for $x > x_{c2} > x_{c1}$. We analyze and discuss in detail x_{c1} and x_{c2} as well as b clump size distributions as a function of V_0, E_{JT} and the arrangement of the alkaline-earth ions. We exhibit several examples of real-space inhomogeneous structures. The spatial autocorrelation of holes (absence of polarons) and of holes with alkaline-earth ions is also elaborated. We compare the effective b bandwidth obtained from simulations which have the intrinsic nanoscale inhomogeneity mentioned above with results from single-site dynamical mean-field theory (DMFT) (Ref. 17) neglecting long-range Coulomb interactions but forcing homogeneity ("annealed disorder") and find very good agreement.

In the final part of this paper (Sec. IV) we discuss some of the approximations made, e.g., the assumption of random distribution of dopant ions, the effect of disorder, and its modeling. We also mention a number of implications of our results for manganites such as Coulomb glass behavior and other signatures of nanoscale inhomogeneities on transport properties. We place our results in the context of the inhomogeneities observed in experiments and suggest some experiments to investigate long-range strain effects. A short description of this work has been published.[24]

II. MODEL AND METHOD

This section contains four parts. In the first part (Sec. II A), the ℓb model[17–19] is briefly described. The second part (Sec. II B) contains a description of the extended ℓb Hamiltonian. A simplified analytical solution for the ground state of the extended ℓb Hamiltonian is presented in the third part (Sec. II C). Finally, the determination of the ground state of the extended ℓb Hamiltonian is described in the final part (Sec. II D).

A. Summary of the ℓb model

The $Mn^{3+,4+}$ ions in $Re_{(1-x)}Ak_xMnO_3$ form a simple cubic lattice (with lattice parameter taken as a, lattice sites indexed by i). Each manganese ion experiences the octahedral environment of oxygen atoms and thus the d states are crystal field split into t_{2g} and e_g orbitals. For the purposes of describing the low-energy physics of manganites one can treat the t_{2g} levels as always occupied by three electrons at every site, with parallel spin because of a strong Hund's rule, and hence replace them by a $S=\frac{3}{2}$, "t_{2g}—core spin," and in the rest of this paper we approximate this as a classical spin, $S\hat{\Omega}$ where $\hat{\Omega}$ is a unit vector. The remaining $(1-x)$ electrons per site

move around among the e_g orbitals with an average hopping amplitude t. However, they have a strong Hund coupling J_H with the core spin, and there is a strong on-site Coulomb repulsion U between the e_g electrons. Furthermore, they have a strong Jahn-Teller interaction with the modes of distortion of the oxygen octahedron surrounding the Mn^{3+} ions. As a consequence of this and phonon dynamics, two types of low-energy effective e_g electronic states called ℓ and b emerge. The polaronic ℓ state is associated with a local lattice distortion in which an e_g electron can get self trapped, with a binding energy E_{JT}. The hopping of the ℓ polaron gets suppressed exponentially by the Huang-Rhys factor η $(=e^{-E_{JT}/2\hbar\omega_0}\approx 1/200$, where ω_0 is the frequency of the local lattice distortion). The reduction arises from the fact that the hop of the polaron from one site to a neighboring one, in addition to the transfer of the electron, involves the relaxation of the lattice distortion at the original site and effecting a similar lattice distortion at the neighboring site and the exponentially small overlap of the corresponding phonon wave functions. On the other hand, as $t \gg \bar{\omega}_0$, e_g electrons can also hop fast among empty, undistorted or weakly distorted sites with essentially the bare amplitude t, leading to the b states. The greatly diminished hopping of the polarons allows for a useful approximation: at temperatures much larger than ηt, the polarons may be considered as static. The effective ℓb Hamiltonian can therefore be written as

$$\mathcal{H}_{\ell b} = -E_{JT}\sum_{i,\sigma} \ell^{\dagger}_{i\sigma}\ell_{i\sigma} - t\sum_{\langle ij\rangle}(b^{\dagger}_{i\sigma}b_{j\sigma} + \text{H.c.}) - J_H\sum_i (\boldsymbol{s}_{i\ell} + \boldsymbol{s}_{ib})\cdot \boldsymbol{S}_i + U\sum_i n_{il}n_{ib} - \mu\sum_i (n_{il}+n_{ib}) - (J_{VDE} - J_{SE})\sum_{\langle ij\rangle}\boldsymbol{S}_i\cdot\boldsymbol{S}_j. \quad (1)$$

Here $\boldsymbol{s}_{i\ell}(n_{i\ell})$ and $\boldsymbol{s}_{ib}(n_{ib})$ are spin (number) operators corresponding to the ℓ and b degrees of freedom at site i and μ is the chemical potential determined from the condition that $\langle n_l + n_b\rangle = 1-x$. The last term contains the "virtual double exchange" ferromagnetic coupling with strength $J_{VDE}\sim x(1-x)t^2/E_{JT}$. This coupling between the neighboring core spins arises from fast virtual hopping processes of the ℓ electron to a neighboring vacant site. J_{SE} is the antiferromagnetic superexchange. The above Hamiltonian treats all the main energy scales that govern manganite physics. The three largest local (strong correlation) energies are the on-site Coulomb or Mott-Hubbard repulsion $U\approx 5$ eV, the Hund's rule ferromagnetic exchange coupling $J_H\approx 2$ eV and the Jahn-Teller energy E_{JT} ($\approx 0.6-1$ eV). The other important interactions are the nearest neighboring hopping $t\approx 0.2$ eV, the doping-dependent virtual double exchange, and the superexchange $J_{SE}\approx 0.01$ eV.

Several simplifying approximations have been made in writing Hamiltonian (1). The first is that the kinetic energy in the Hamiltonian is "orbitally averaged," i.e., the hopping amplitude t represents an average over the possible orbital configurations at the two pertinent sites. Second, there are no cooperative/long-range lattice effects, i.e., no intersite polaron correlations. Third, the virtual double exchange has been approximated as a homogeneous interaction J_{VDE} ; in reality it acts only between pairs of sites where one is occupied by a polaron and the other is empty. Fourth, the Jahn-Teller interaction has been included only to the extent that it leads to the formation of polarons. But its merit is that all the important energy scales governing manganite physics are included in Eq. (1), at least in an approximate fashion. Much of the previous work on manganites is based on simplified models[9,25,26] that neglect one or more of these energy scales.

Hamiltonian (1) closely resembles the Falicov-Kimball model (FKM) (Ref. 27); in fact, for $J_H\to\infty$ and at $T=0$, when all the spins are completely ferromagnetically aligned, it is the same as the FKM. The model was solved[17–19] using the dynamical mean-field theory.[28] It is successful in capturing the colossal magnetoresistance effect, the ferromagnetic insulating state found in low bandwidth manganites, the systematics of the role of R and Ak ion radii, etc. The key point is that for small doping x the majority of the e_g electrons get localized as ℓ polarons. Because of the strong on-site Coulomb interaction U (the largest energy scale in the problem) the b electrons avoid the polaronic sites, and this reduces the effective half bandwidth of the b states from its bare value D_0 to D_{eff} which is strongly (x) dependent. At zero temperature with $U, J_H\to\infty$ and a ferromagnetic ordering of the core spins, the effective half bandwidth is given by[17]

$$D_{eff} = \sqrt{x}D_0. \quad (2)$$

Thus, at low doping, the effective band bottom is above the polaronic energy level $-E_{JT}$ and therefore the b band is unoccupied and the chemical potential μ is pinned at $-E_{JT}$. Clearly, beyond a critical doping x_c given by

$$x_c = \left(\frac{E_{JT}}{D_0}\right)^2, \quad (3)$$

the b states begin to be occupied, leading to a insulator to metal transition. Furthermore, for $x>x_c$, starting from the metallic state at $T=0$, the effective bandwidth reduces from its zero temperature value with increase in temperature. This is because the hopping of the b electrons is strongly inhibited on account of their Hund coupling J_H to the thermally disordered core spins. Hence one gets a thermally induced ferrometal to parainsulator transition when the b band moves above E_{JT}. For T near T_c, the application of an external magnetic field causes the core spins to align and thus increases the effective bandwidth, leading to increase in the number of thermally excited carriers by orders of magnitude. This causes colossal magnetoresistance. Away from the "orbital liquid regime," the ℓ-b model can be extended in a straightforward way to include charge and orbital order particularly near $x=0.5$.[29,30]

The work cited above did not address the issue of electronic inhomogeneities. In fact, an effective homogeneous state was *assumed* in the dynamical mean-field solution. This is a drastic assumption because from previous work on the Falicov-Kimball model[31] [and as confirmed by our computer simulations (see Fig. 1)] the ground state of ℓb Hamiltonian (1) (for the parameter ranges discussed above) is known to be *a macroscopically phase-separated state* due to the strong on-site Coulomb correlation U. All the polarons cluster on

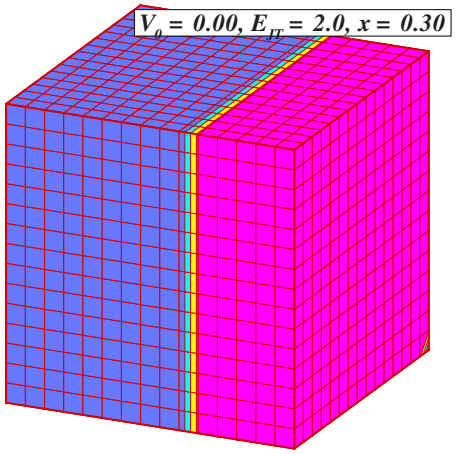

FIG. 1. (Color online) "Macroscopic phase separation" in the ℓb model in absence of long-ranged Coulomb interaction. The lighter regions correspond to holes that form a large clump (with occupied b states), the darker regions are occupied by ℓ polarons. This simulation is performed with a cube of size $16\times16\times16$.

one side of the box; this allows band states (b) to optimize their kinetic energy by moving among the vacant "hole" sites in the other part of the box. But the two portions have drastically different electron densities. The motivation for the homogeneity assumption made in the DMFT work was that the phase separation will of course be prevented by the long-ranged Coulomb interactions which are always present in the real system. In this work, we extend the ℓb model to include long-ranged Coulomb interactions to address the issue of electronic inhomogeneities and to check to what extent the DMFT homogeneity assumption is valid.

B. Extended ℓb Hamiltonian

The Hamiltonian is most conveniently developed in terms of hole operators $h_i^\dagger = \ell_i$, which create vacant sites not occupied by polarons. A hole carries a positive unit charge. The charge is counterbalanced by the Ak^{+2} ions which have a negative unit charge. The Ak ions occupy the sites $(\frac{l}{2},\frac{m}{2},\frac{n}{2})$, where l,m,n are odd integers (mimicking the perovskite-type structure of manganites); the number of Ak ions is equal to xN (N is the number of sites in the model), and they are placed randomly on the lattice sites indicated. In the orbital liquid regime[17–19] with large Hund coupling and on site Coulomb repulsion discussed above, and at $T=0$, corresponding to a fully ferromagnetic alignment of the core spins (spin drops out of the problem in this limit), the extended ℓb Hamiltonian for fixed particle number is given by

$$\mathcal{H}_{\ell b}^{ext} = E_{\rm Ak} + \sum_i \Phi_i \hat{q}_i + V_0 \sum_{\{ij\}} \frac{1}{r_{ij}} \hat{q}_i q_j - t \sum_{\langle ij\rangle} (b_i^\dagger b_j + b_j^\dagger b_i) + E_{JT} \sum_i h_i^\dagger h_i, \tag{4}$$

where

$$\hat{q}_i = h_i^\dagger h_i - b_i^\dagger b_i \tag{5}$$

is the charge operator at hole site i (in units of $|e|$), $E_{\rm Ak}$ is the Ak-Ak electrostatic interaction energy (a fixed number for a given realization of Ak distribution in the lattice), Φ_i is the Coulomb potential at the hole site i due to Ak ions, V_0 is the strength of the Coulomb interaction between nearest-neighbor holes (of the order of 0.02 eV, $V_0 \approx 0.01t - 0.1t$, see discussion below), and r_{ij} is the distance between holes i and j in units of the lattice constant. Each hole has an energy penalty of E_{JT}. The sum $\{i,j\}$ is over all pairs of hole sites, while $\langle ij\rangle$ denotes a sum only over nearest-neighbor hole sites. The site charge operators satisfy the constraint

$$\sum_i \langle \hat{q}_i \rangle = xN. \tag{6}$$

The $U\to\infty$ constraint implies that the b electrons can only move among hole sites, where $h_i^\dagger h_i = 1$.

Hamiltonian (4) embodies the competition between long-range Coulomb interaction which works to keep the holes as far apart as possible, while the kinetic energy of band electrons promotes the formation of "clumps." A clump is a collection of hole sites, each member of which can be reached from any other member via a sequence of nearest-neighbor hops which visit only the members of the clump. Thus every configuration of holes can be broken up into a set of clumps where each hole belongs to only one clump. Site delocalized electronic b states are possible in a clump that has more than one member (a one member clump is called a "singleton"). The kinetic-energy gain can possibly promote an ℓ polaron to occupy the b state in the clump leading to an electron puddle, which creates an additional hole in the system at the site from which the ℓ polaron is removed, which changes the electrostatic energies, etc. Thus the number of holes and number of band electrons is not individually conserved, but only the constraint [Eq. (6)] is satisfied. The key question is: what is the ground state of the Hamiltonian for a realization of the random distribution of the Ak ions? The determination of this ground state requires an optimization of the number of holes and their distribution (or equivalently, the configuration of the on site ℓ polarons, which exist at sites where the holes are not there), as well as the clump structure, the associated b states, and their occupancy (constituting the b puddles surrounded by the ℓ polarons) so as to achieve the lowest energy of Hamiltonian (4). An exact solution of this problem is beyond the available techniques of correlated electron theory so approximations have to be resorted to. In this paper we explore two alternate ways; the first one is essentially analytic (and very approximate), while the second one is a full scale numerical treatment.

C. Simplified analytic treatment

A simple analytical approximation for the ground state becomes possible if we assume that the Ak ions are distributed homogeneously in space, i.e., model the charge of the Ak ions as a "jellium." The approximation involved is a variational calculation with an assumed ground state as shown in Fig. 2, where clumps of size R (volume R^3) are

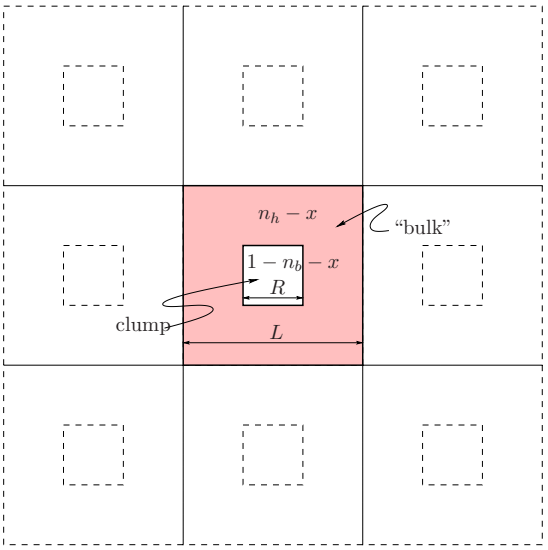

FIG. 2. (Color online) Schematic of the ground state used in the analytical calculation of Sec. II C. Phase separation takes the system to two distinct type of regions called the bulk (regions with ℓ polarons) and the clump. The dashed lines indicate the assumed periodic nature of the clump distribution—clumps of size R (volume R^3) are assumed to be arranged in a periodic fashion (period L) with intervening bulk regions. Site delocalized electronic states are found in the clumps. The initial hole density is x (also equal to the background negative charge density). The charge density in the clump is $(1-n_b-x)$ and that in the bulk is n_h-x. n_b is the fraction of electrons that are promoted to delocalized states, and n_h is the fraction of holes created in the bulk. The fractions x, n_b, and n_h are related via charge balance.

taken to be spaced periodically with a spacing L. The regions between the clumps—the "bulk," is taken to have concentration of holes n_h (the concentration of holes in the clump is, of course, unity). Charge conservation gives

$$(1-n_b)R^3 + n_h(L^3 - R^3) = xL^3, \tag{7}$$

whence

$$n_h = \frac{\alpha^3 x + (b-1)}{\alpha^3 - 1}, \tag{8}$$

with $\alpha = L/R$. Clearly, the charge density ρ_C in the clump is $(1-n_b-x)$ and that in the bulk ρ_B is n_h-x, i.e.,

$$\rho_C = 1 - n_b - x, \quad \rho_B = n_h - x = -(1-n_b-x)\frac{1}{\alpha^3 - 1}. \tag{9}$$

Associated with this charge distribution, there is an electrostatic energy (per "unit cell" of volume $L^3 = \alpha^3 R^3$) given by

$$E_{ES}(n_b, \alpha, R) = V_0 \mathcal{E}(n_b, \alpha, R/a), \tag{10}$$

where a is the lattice parameter of the underlying atomic lattice, $\mathcal{E}(n_b, \alpha)$ is the "Madelung function" accounting for the net electrostatic energy in the system. Since a total number of $n_b R^3$ polarons have been promoted to delocalized b electrons, there is a loss of polaron energy proportional to this number, i.e.,

$$E_P(n_b, \alpha, L) = E_{JT} n_b R^3. \tag{11}$$

Finally, there is the delocalized kinetic energy of the electrons, which is expected to be of the form

$$E_{KE}(n_b, R) = t\mathcal{K}(n_b, R), \tag{12}$$

where $\mathcal{K}$ is a function of n_b, R. It can be evaluated by finding the kinetic energy of $b_b R^3$ electrons in a clump of size R^3. Note that we do not take E_{KE} to go as $1/R^2$ as might be expected from a free-electron picture since the lowest energy that can be attained a tight binding scenario is bounded below by $-6t$ (for a cubic lattice).

Putting everything together, we get

$$E_{tot}(n_b, \alpha, R) = E_{ES}(n_b, \alpha, R) + E_P(n_b, R) + E_{KE}(n_b, R). \tag{13}$$

We need to minimize this energy as a function of n_b, α, and R; this will give us the clump size, spacing, and charge distribution.

In the remainder of this section R stands for a dimensionless number (clump size normalized by lattice parameter a). Similarly charge densities are all dimensionless. We shall now proceed to estimate the different energy functions noted above.

We estimate the electrostatic energy by assuming the box is "spherical." In this case the total charge in the box is zero, and hence the electric field *outside the sphere vanishes*, hence to a very crude approximation one box does not affect the energy of the neighbor. This is expected to be quite reasonable when the Ak ions are distributed homogeneously (as we have assumed in this calculation) since the electrostatic interaction is expected to be well screened. With these assumptions, we find

$$E_{ES}(n_b, \alpha, R) = \frac{(4\pi)^2}{45} V_0 (1 - n_b - x)^2 R^5 f(\alpha), \tag{14}$$

where $f(\alpha)$ is the function

$$f(\alpha) = 1 + \frac{1}{\alpha}\left(\frac{(\alpha^6 - 5\alpha^3 + 9\alpha - 5)}{(\alpha^3 - 1)^2} - \frac{5(\alpha-1)^2(\alpha+2)}{(\alpha^3 - 1)} + 5(\alpha - 1) \right). \tag{15}$$

The function f is such that $f(1)=1$ and $f(\infty)=6$, a very slowly varying function of α and always of order unity.

The polaron energy (again for a spherical clump) is

$$E_P(n_b, \alpha, L) = \frac{4\pi}{3} E_{JT} n_b R^3. \tag{16}$$

The estimation of the kinetic energy entails probably the crudest approximation of this analysis. We assume that the density of states is "flat"

$$g(\epsilon) = \frac{1}{12t}, \quad -6t \le \epsilon \le 6t. \tag{17}$$

With this assumption we estimate the kinetic energy (for a spherical clump) to be

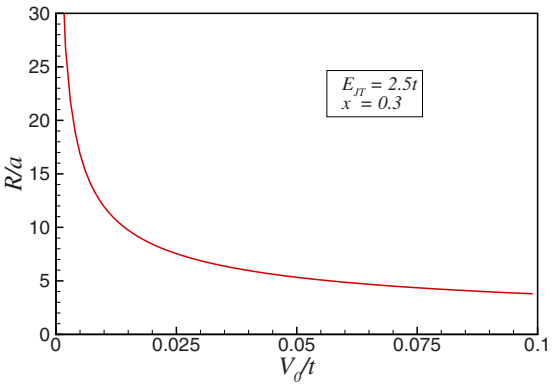

FIG. 3. (Color online) Electron puddle size (normalized by lattice parameter a) as a function of the Coulomb interaction parameter V_0 (normalized by t) for $E_{JT}=2.5t$ and $x=0.3$.

$$E_{KE}(n_b,R) = -\frac{4\pi}{3}R^3(6t)n_b(1-n_b). \tag{18}$$

The total energy is given by

$$E(n_b,\alpha,R) = \frac{4\pi}{3}\left(\frac{4\pi}{15}V_0(1-n_b-x)^2R^5f(\alpha) + E_{JT}n_bR^3 - 6tn_b(1-n_b)R^3\right). \tag{19}$$

The analysis of the minima of the above function shows that $E_{JT}<6t$ *is a necessary condition* for the existence of a clump. If $E_{JT}>6t$, then the coefficients of R^5 and R^3 are both positive (for any value of b) and hence R will vanish for energy minimum. Inspecting Eq. (7) we see that this will result in a homogeneous distribution of the holes in the "bulk" equal to the cation charge density—the bulk becomes neutral.

We now consider $E_{JT}<6t$. Furthermore, (1) the b electron density in the clump is determined by chemical potential balance. For the case of a flat band density of states, this will imply that the "chemical potential" is E_{JT} and

$$\int_{-6t}^{-E_{JT}} \frac{1}{12t}de = n_b \Rightarrow n_b = \frac{1}{2}\left(1-\frac{E_{JT}}{6t}\right). \tag{20}$$

(2) The factor α is determined from the condition that the hole density in the bulk vanishes [charge conservation resulting in Eq. (8)]

$$\alpha^3 = \frac{1-n_b}{x}. \tag{21}$$

Within this framework, we minimize Eq. (19) with respect to R to obtain

$$R^2 = \frac{9n_b[6t(1-n_b)-E_{JT}]}{4\pi f(\alpha)V_0(1-n_b-x)^2}. \tag{22}$$

Note that the clump size varies as $1/\sqrt{V_0}$.

We take $E_{JT}\approx 2.5t$, $x\approx 0.3$ to study the clump size as a function of V_0. The result is shown in Fig. 3. For these values, the centers of the clumps are spaced at a distance of about two and a half times the clump size ($\alpha=1.33$). A reasonable estimate of V_0 in manganites is about $0.1t$ (V_0 is likely to be between 0.01 and 0.1, see discussion below). In this range we see that the clump size is between 5 and 10 lattice spacings (taking $a=5$ Å, we get $R=2-5$ nm), in surprisingly good agreement with available experiments. We must emphasize that we really do not have tight control of the constants (such as $9/4\pi$ appearing in the equation for R). However, the main point that we learn is that the clump size is a few lattice spacings, much as what the Coulomb interaction is expected to do. We note here that there has been a recent calculation[32] of "phase separation" in doped manganites adding in Coulomb effects to the two fluid ℓ-b model of Ref. 19 along lines similar to those discussed above. However, that calculation does not uncover the dependence of the clump size on the long-ranged Coulomb interaction as we have done here.

We note again that the key assumption of the above analysis is the homogeneous distribution of the Ak ions. A more realistic solution that takes into account the inhomogeneous random distribution of the Ak ions requires a full scale numerical treatment of Eq. (4), and we turn to this next.

D. Approximate determination of the ground state

The key approximation that permits a numerical determination of the ground state of Hamiltonian Eq. (4) is a Hartree-like treatment of the Coulomb interactions between the b electrons. This allows us to treat all the electrostatic energy contributions in a classical fashion, i.e., replace the site charge operators $\hat{q}_i$ by their expectation values q_i in the ground state $|\ \rangle$:

$$q_i = \langle\ |h_i^\dagger h_i - b_i^\dagger b_i|\ \rangle. \tag{23}$$

In the absence of b states the problem reduces to the Coulomb glass problem[23,33]—a fully classical problem. The presence of the b states makes the system a new kind of quantum Coulomb glass—the h-b glass—with *coexisting localized and delocalized states*, in contrast to usual quantum Coulomb glasses.[34] Since the Ak ions are randomly distributed, and in addition the density of b electrons is very low, a Hartree approximation is likely to be reasonably accurate. We do indeed find (see below) that the interaction is well screened and the charge distribution is almost homogeneous at scales larger than a few lattice spacings.

Our method of determination of the ground state is based on a generalization of the method previously used in finding ground states of the classical Coulomb glass.[35,36] Here, the ground state is obtained by starting from a trial configuration (usually a random state) and "performing" transfers of electrons that lower energy until no transfer is possible that can lower the energy. In the classical Coulomb glass each transfer involves moving an electron from its current position to a vacant site, creating a particle hole "excitation." To follow a strategy similar to the one above in the present context, we investigate the energetics of possible transfers in the h-b glass.

The following definitions are useful to understand excitations in the h-b glass. Each clump α has many delocalized

one particle levels (obtained by diagonalizing the kinetic energy on this clump); we label these one particle levels by r and denote their kinetic energy by $\epsilon_{\alpha,r}$. The operator

$$b^{\dagger}_{\alpha,r} = \sum_{i(\alpha)} \Psi_i^{\alpha,r} b_i^{\dagger} \tag{24}$$

creates a b electron in the rth band state of the clump α, where $\Psi_i^{\alpha,r}$ is the associated single particle wave function spread out over the clump [i runs over all hole sites in the clump α as indicated by $i(\alpha)$]. Clearly, for a hole at site i

$$q_i = 1 - \sum_r |\Psi_i^{\alpha,r}|^2 \theta(\mu - \epsilon_{\alpha r}). \tag{25}$$

Here α is the clump to which the hole i belongs, and r runs over all the *occupied* band states in the clump α. The potential ϕ_i at hole site i is defined as

$$\phi_i = V_0 \sum_{j \neq i} \frac{1}{r_{ij}} q_j. \tag{26}$$

Consider, for a given x, a configuration containing N_h holes and N_b band electrons (obviously, $\Sigma_i q_i = N_h - N_b = xN$), with N_c clumps. The extra energy E_i^h in the system due to the addition of a hole at a hole-vacant site i *without changing the clump structure* is

$$E_i^h = \Phi_i + \phi_i + E_{JT}. \tag{27}$$

The addition of a hole can, in general, change the clump structure since the new hole can modify existing clumps or create new clumps. If the modified clumps contain band electrons, then their energies will change. We ignore these effects in writing Eq. (27). A similar definition of $E^b_{\alpha,r}$, the energy increment for the addition of a band electron in the vacant-band state α, r, is

$$E^b_{\alpha,r} = \epsilon_{\alpha,r} - \sum_i (\Phi_i + \phi_i) |\Psi_i^{\alpha,r}|^2 + V_0 \sum_{\langle i,j(i \neq j) \rangle} \frac{1}{r_{ij}} |\Psi_i^{\alpha,r}|^2 |\Psi_j^{\alpha,r}|^2, \tag{28}$$

where i,j run over all the hole sites in clump α. The definitions E_i^h and $E^b_{\alpha,r}$ serve as the equivalent of the "single particle levels" in the present context (Hartree approximation).

These definitions allow us to determine energies of excitations in the h-b glass corresponding to the creation/annihilation of holes or b/ℓ electrons. Strictly, the clump structure changes in an excitation; as mentioned earlier we ignore this and our excitations are "frozen-clump excitations."

Three types of excitations are possible in the h-b glass:

(1) "ℓ-h" excitations: here a hole-occupied site j obtains an electron from a hole-vacant site (ℓ occupied site) i. The energy for this excitation is

$$\mathcal{E}^{\ell\text{-}h}_{i;j} = E_i^h - E_j^h - \frac{V_0}{r_{ij}}. \tag{29}$$

This type of excitations can affect the clump structure. This arises from the fact that the clump structure is determined by the position of the holes.

(2) "ℓ-b" excitations: here a hole-vacant site i (containing an ℓ electron) donates an electron to a vacant band state (α, r). The energy of this type of excitation is

$$\mathcal{E}^{\ell\text{-}b}_{\alpha,r;i} = E^b_{\alpha,r} + E_i^h - V_0 \sum_j \frac{1}{r_{ij}} |\Psi_j^{\alpha,r}|^2, \tag{30}$$

where j run over all the hole sites in clump α. Again, this type of excitation can change the clump structure. It must be noted that the reverse of this process is also a possible excitation (a b-ℓ excitation), in that a band electron annihilates a hole, the energy of which is negative of Eq. (30). Again, since both ℓ-b and b-ℓ excitations change the position of the holes, they can affect the clump structure.

(3) "b-b" excitations: Here a b-electron transfers from (α, r) b state to the vacant (β, s) b state. The energy of this excitation is

$$\mathcal{E}^{b\text{-}b}_{\beta,s;\alpha,r} = E^b_{\beta,s} - E^b_{\alpha,r} - V_0 \sum_{i,j} \frac{1}{r_{ij}} |\Psi_i^{\beta,s|}|^2 |\Psi_j^{\alpha,r|}|^2, \tag{31}$$

where i,j run over β and α (the last term requires obvious modifications if $\alpha = \beta$). Note that this type of excitation will not affect the clump structure since it does not affect the position of the holes.

For a given doping, the ground state is obtained in two stages. In the first stage, b states are not accounted for and the classical Coulomb glass ground state of the holes in presence of the electrostatic potential from the Ak ions is obtained. This is achieved by performing a series of ℓ-h excitations until a minimum energy configuration is achieved. In the second stage, starting from the classical Coulomb glass state, all possible excitations are performed iteratively. Each iteration consists of the following steps:

(1) Find best excitation: from the definition of the single particle levels E_i^h, $E^b_{\alpha,r}$, and the excitation energies defined above, the best possible excitation (the one that reduces the energy the most) is determined.

(2) Perform the excitation: if it is an ℓ-h excitation, then one hole is removed and one is added. If it is an ℓ-b or b-ℓ excitation, then either a hole is removed or added. If it is b-b excitation, holes do not change. Thus, ℓ-h and ℓ-b excitations change the clump structure.

(3) Update clump structure: if the clumps with occupied band states are not disturbed, then no update is required. If some of the clumps have been disturbed, then the intersection of the old clumps and new clumps is found, and electrons are distributed in the new clumps so that the charge distribution is as close as possible to that of the previous distribution. After update, the number of band electrons must be same as before, unless isolated holes in the new clump structure are annihilated by band electrons. All energies are recalculated on update.

Iterations are carried out until an energy minimum is achieved. It must be noted that the ground state that we obtain is based on single particle excitations. In general, the stability of the ground state must be checked for two (and multi) particle excitations.[36] This process is computationally intensive. The correctness of the ground state obtained in our case is affirmed by the energies of the highest occupied states

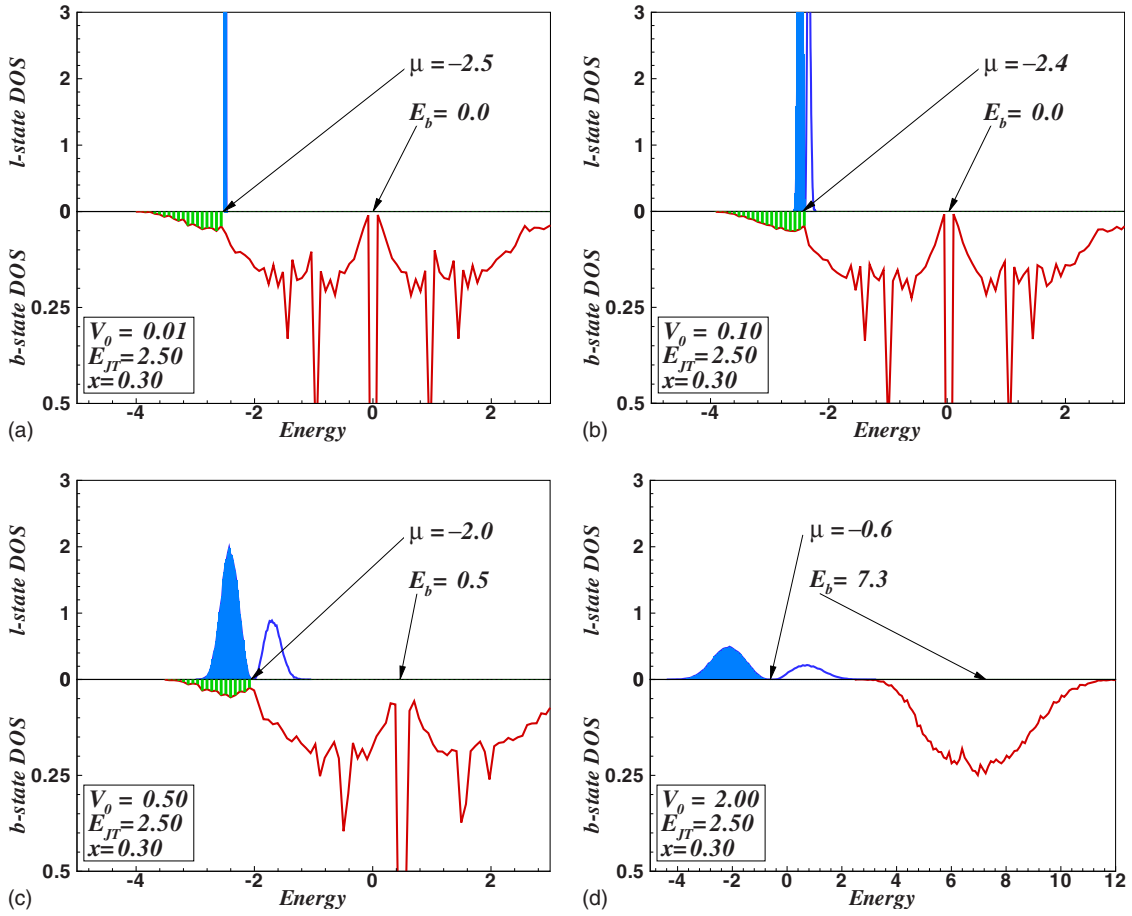

FIG. 4. (Color online) Density of states (DOS) of ℓ polarons and b electrons, where their respective energies are defined by Eqs. (27) and (28). The occupied states are shaded. The chemical potential μ and the center of the b-band E_b are indicated. The different panels (a)–(d) show the variation in the densities of states as a function of V_0 for $E_{JT}=1.0$ and $x=0.3$. The polaron density of states shows a Coulomb gap at the chemical potential for all values of V_0 including $V_0=0.01$ [graph (a), top-left].

of the ℓ electrons and the b electrons—if the ground state calculation is correct, then the highest occupied states of both types of electrons will correspond to the chemical potential μ. We have never found serious violation of this criterion in several ten thousand simulations; we therefore believe that our scheme is robust enough to determine the ground state of the h-b glass.

The electrostatic energy is calculated using the Ewald technique[37] using fast Fourier transform routines made possible by the use of periodic boundary conditions. The other computationally intensive step is the calculation of energies and wave functions of the b states in a clump. This is the most CPU intensive step which limits the size of the simulation cell. The size of the cell that can be calculated depends on the doping. For $x=0.2$ we have calculated with cells as large as $20\times20\times20$.

Some other points regarding our simulations may be noted. First, the strong correlation U that induces many body effects is treated almost exactly (since U in the real system is very large, the $U=\infty$ limit is accurate); the b-electron quantum dynamics is treated almost exactly (b electrons do not hop to sites with ℓ polarons). In our calculation, the long-ranged Coulomb energy (within the Hartree approximation) is treated accurately using Ewald techniques (as mentioned above), and no further approximations are made in the calculation of the long-ranged electrostatic energy. Further, we note that the Hamiltonian we study and the method we develop here to find the ground state is a generalization (both model and method) of the quantum Coulomb glass. The key point is that our model consists of two types of electronic states, one localized polaronic (classical) and other delocalized bandlike (quantum), and our treatment accounts for both of these on an equal footing.

III. RESULTS

This section contains the results of our study of the extended ℓb Hamiltonian (4). The key parameters in the Hamiltonian are energies t, E_{JT}, V_0 and the doping x. The hopping amplitude t is taken as the basic energy scale, and E_{JT} and V_0 henceforth stand for the dimensionless values of the Jahn-Teller energy and the long-range Coulomb interaction strength parameter normalized by t. Further all length scales are normalized by the lattice parameter a. We have checked for the size dependence of the results and found that results for cubes larger than $8\times8\times8$ are essentially independent of the size. We checked densities of states, clump size distribution, etc., calculated in some cases up to cubes of size 20

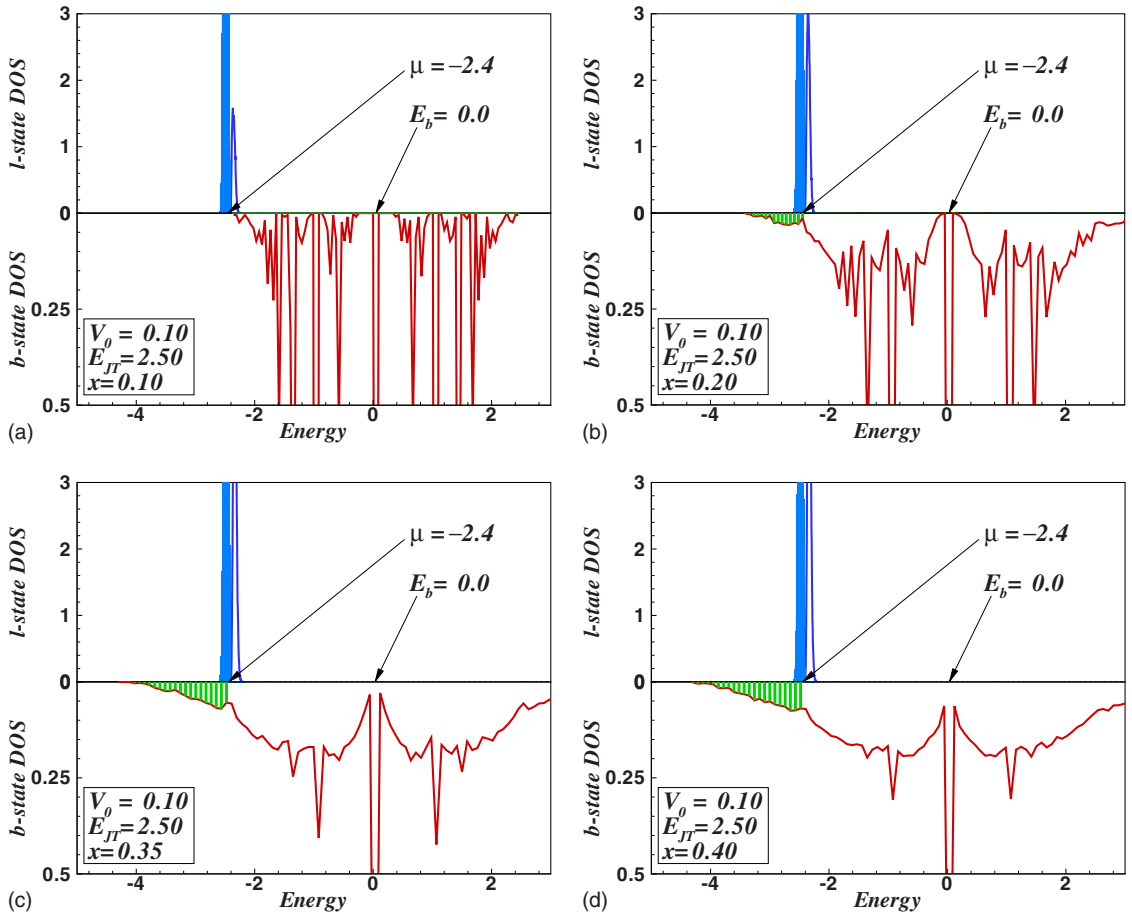

FIG. 5. (Color online) DOS of ℓ polarons and b electrons, where their respective energies are defined by Eqs. (27) and (28). The occupied states are shaded and the chemical potential is marked by μ. The center of the b-band E_b is also indicated. The different panels (a)–(d) show the variation in the densities of states as a function of x for V_0=0.1 and E_{JT}=2.5. It is evident that the b bandwidth increases with increasing doping x.

$\times 20 \times 20$. We found that results followed essentially the same trends, independent of size. All the results shown here are averages from calculations obtained with one hundred random initial conditions using $10 \times 10 \times 10$ cells unless stated otherwise.

The density of states obtained from simulations is discussed first. The energies of the single particle states are defined in Eq. (27) for a hole (with a similar expression for an ℓ polaron) and Eq. (28) for the band electron. Figures 4–6 show plots of densities of states for various values of V_0, E_{JT}, and x with the chemical potential μ and b band center E_b indicated in each case. Figure 4 shows the variation in the density of states with the parameter V_0, Fig. 6 shows the variation in the density of states with the parameter E_{JT} (V_0 and x fixed) and Fig. 5 shows the effect of doping on the density of sates for fixed values of V_0 and E_{JT}. From a study of these figures we observe the following: the chemical potential is given by

$$\mu = -E_{JT} + A(x)V_0, \tag{32}$$

where $A(x)$ is a "very weak" function of x, with size of order unity; the physics behind this will be discussed later.

We now discuss the ℓ polaron states: as discussed in Sec. II B, the polarons with long-range Coulomb interaction form a Coulomb glass.[23] A Coulomb glass possesses a "soft gap" at the chemical potential μ, in that the density of states scales as

$$\rho_\ell(\epsilon - \mu) \sim (\epsilon - \mu)^2, \tag{33}$$

as is seen in Fig. 4. It is also evident that the width (energy spread) of the two lobes in the polaron density of states separated by the chemical potential increases with increasing V_0. Thus the polaron energies do not have a single value $-E_{JT}$ but have a distribution whose width scales with V_0. The energy spread arises out of fluctuations in the local electrostatic potential. This is the basic reason why though the polarons form a narrow band, there are no heavy fermionlike specific-heat effects. The occupied polaron states (indicated by shaded portion below the chemical potential in Fig. 5) per unit volume are proportional to $(1-x)$ for large values of $V_0(\gtrsim 1.0)$. For lower values of the V_0, the occupied spectral weight is less, owing to the fact that some electrons are promoted to the b states. The effect of E_{JT} on the polaron density of states is shown in Fig. 6. Since E_{JT} determines the chemical potential via Eq. (32), it does not affect the width

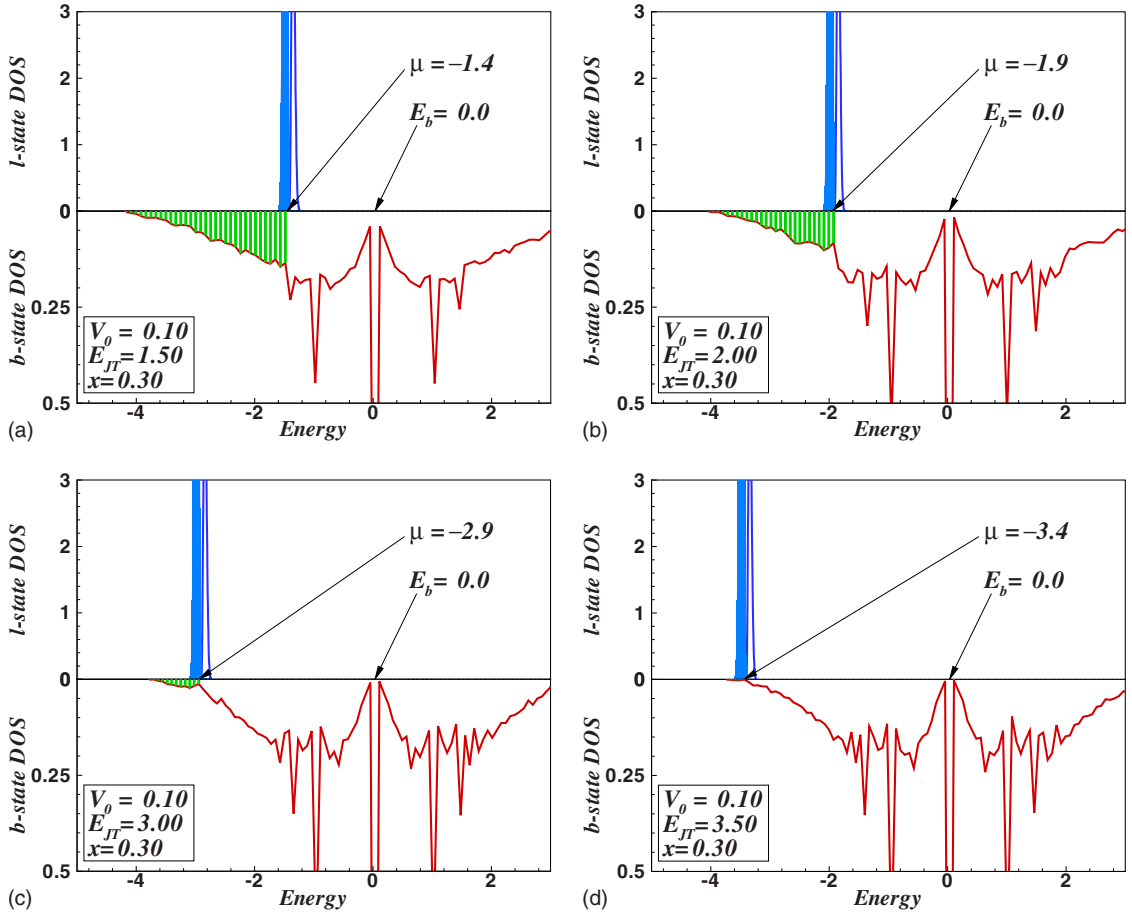

FIG. 6. (Color online) DOS ℓ polarons and b electrons, where their respective energies are defined by Eqs. (27) and (28). The occupied states are shaded and the chemical potential is marked by μ. The center of the b-band E_b is also indicated. The different panels (a)–(d) show the variation in the densities of states as a function of E_{JT} for V_0=0.1 and x=0.1. The main effect of E_{JT} is to determine the chemical potential. E_{JT} does not affect width of the polaron density of states. The bandwidth of the b band is not strongly affected by E_{JT}, while the occupancy is strongly affected.

of the distribution but only affects the ℓ occupancy (amount of spectral weight in each lobe).

Next, we turn to the b electron density of states. Several points may be noted. First, it is clear from Fig. 4 that for $V_0 \lesssim 1.0$, the b band is centered at $E_b = B(x)V_0$ [$B(x)$ is of order unity]. The b band center is independent of E_{JT} (see Fig. 6). Second, as is evident from Fig. 5, the bandwidth of the b states increases with increasing x (in fact, as $\sim\sqrt{x}$ as we shall discuss below) and again essentially independent of V_0 (Fig. 4) as well as of E_{JT} (Fig. 6). Finally, the number of occupied b states (shown by shaded region in the figures) decreases with increasing V_0 and E_{JT}.

The physics underlying these observations may be understood by studying the real-space structure of the ground state, for example, by studying the positional correlation of the holes present in the system (including the holes that appear due to promotion of the ℓ polarons to b electrons as well as the ones already present due to doping). Figure 7 shows both the h-Ak and the h-h correlation functions, which measure, respectively, the probability of finding a hole at a relative distance r from an Ak ion or from another hole. (Note that the Ak ions are placed randomly in the A sites of the perovskite lattice.) If the system were purely random, the probability for any given value of r will be equal to the doping level x. When V_0 is small (V_0=0.01 in Fig. 7), we see the hole-hole correlation function reaches a plateau at a distance $r \gtrsim 2$ with a value larger than x. This latter is because of the increased number of holes in the system due to ℓ polaron to b electron promotion. At larger V_0, the plateau in the hole-hole correlation function appears at x. The hole-Ak ion correlation function reaches a plateau of x, independent of V_0, as expected. The most important feature of the correlation function appears at $r \lesssim 2$. We see that the probability of finding a hole in the neighboring shells is nonzero and is highest at $r=\sqrt{3}$. Further, the probability of finding the Ak ions near the hole is also increased although the increase is smaller than that of finding a hole. This suggests that there is a natural clustering tendency in the h-b glass where the holes tend to cluster around Ak ions. Clearly, this is due to their opposite charge causing gain in electrostatic energy. However, the competing, repulsive electrostatic energy between the holes contributes to control this clustering tendency. Since the distance between the Ak ions and holes is smaller than that between two ℓ polarons, the clustering of holes near Ak ions will offset the energy penalty of ℓ polarons coming together—the short (angstrom sized) clustering scale is result

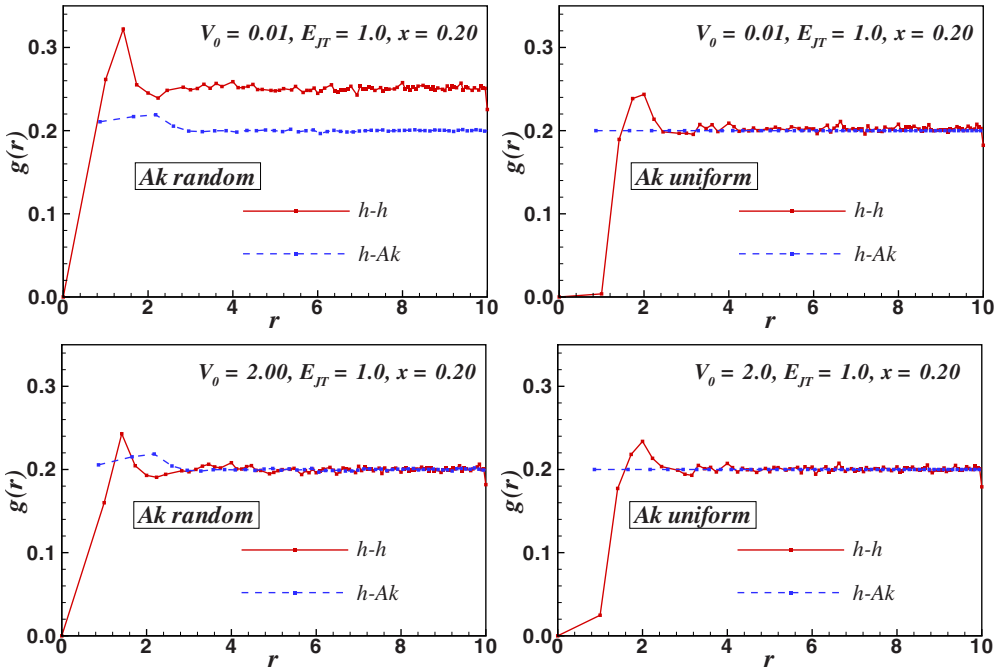

FIG. 7. (Color online) Position correlation function for h-h and h-Ak. The figures in the left column are for random distribution of Ak ions, while those in the right column are for uniform distribution of Ak ions (uniform distribution means that the total charge of the Ak ions is distributed equally among the Ak sites). The result is from simulations with a $20\times20\times20$ cube (for a single realization of the random distribution of the Ak ions in the left-side graphs).

of this competition. Strong screening effects are evident in the correlation functions of Fig. 7—the correlation functions reaches a plateau at about 2–3 lattice spacings.

The observations above allow us to obtain the chemical potential of the system. The hole clustering caused by the hole-Ak ion interaction causes an additional effective electrostatic potential at an ℓ electron site which can be written as $A(x)V_0$, where $A(x)$ is a (here undetermined) doping-dependent factor of order unity. The quantity $A(x)V_0$ can be interpreted as the average electrostatic potential at ℓ polaron sites. The actual energies at the sites fluctuates about the mean total energies of the ℓ polarons given by $-E_{JT}+A(x)V_0$. From the Coulomb glass problem it is known that the chemical potential will be equal to the average energy[23,33] and Eq. (32) follows.

We now discuss the energetics and the nature of the b states, since the transport properties depend crucially on the nature of the b states and whether they are occupied. In case they are not occupied or if all the occupied b states are localized, the system is an insulator; on the other hand if extended b states are occupied one has a metal. We summarize our results in this regard and compare them where ever possible with those obtained in single-site DMFT.[17–19]

The hole site has an average electrostatic potential energy $B(x)V_0$ where $B(x)\approx1$; this follows from arguments very similar to those used earlier for the electrostatic (Hartree) energy of the ℓ-polaron sites. Since the b electrons occupy clumps consisting of hole sites, they too sense this average repulsive potential $B(x)V_0$ and thus the band center E_b shifts to this value (as is seen in the simulation, see Figs. 4–6). The simulations indicate that the effective bandwidth D_{eff} of the b states depends only on the doping x. To understand this result, we calculated D_{eff} as a function of x using clumps obtained from a Coulomb glass calculation of the holes including the random distribution of the Ak ions (thus the calculation was performed with only ℓ-h excitations). The result of this calculation is shown in Fig. 8 along the DMFT result for the bandwidth. It is evident that the agreement is excellent for a wide range of x. Note that the half bandwidth is provided by the clump structure determined by long-ranged Coulomb interactions and the *random distribution* of the Ak ions which induce the clustering tendency of holes around them (as discussed above). Thus the result for the effective bandwidth [Eq. (2)] seems to arise out of two key factors: (a) the large U limit which disallows simultaneous b and ℓ occupancy, and (b) the clumps of holes induced by the random distribution of the Ak ions. This is interesting since it implies

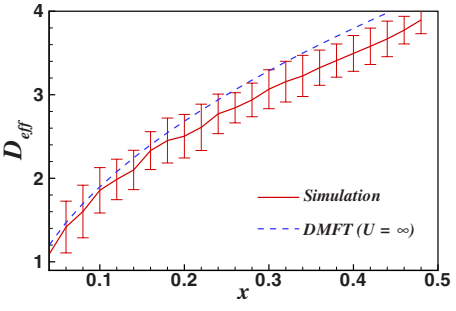

FIG. 8. (Color online) The effective half bandwidth D_{eff} obtained from simulations compared with the DMFT prediction [Eq. (2)]. The half bandwidth in the simulation is calculated by using the clump structure obtained by minimizing the energy of the Coulomb glass. One hundred initial configuration are averaged over to obtain the simulation curve with the standard deviation bars indicated.

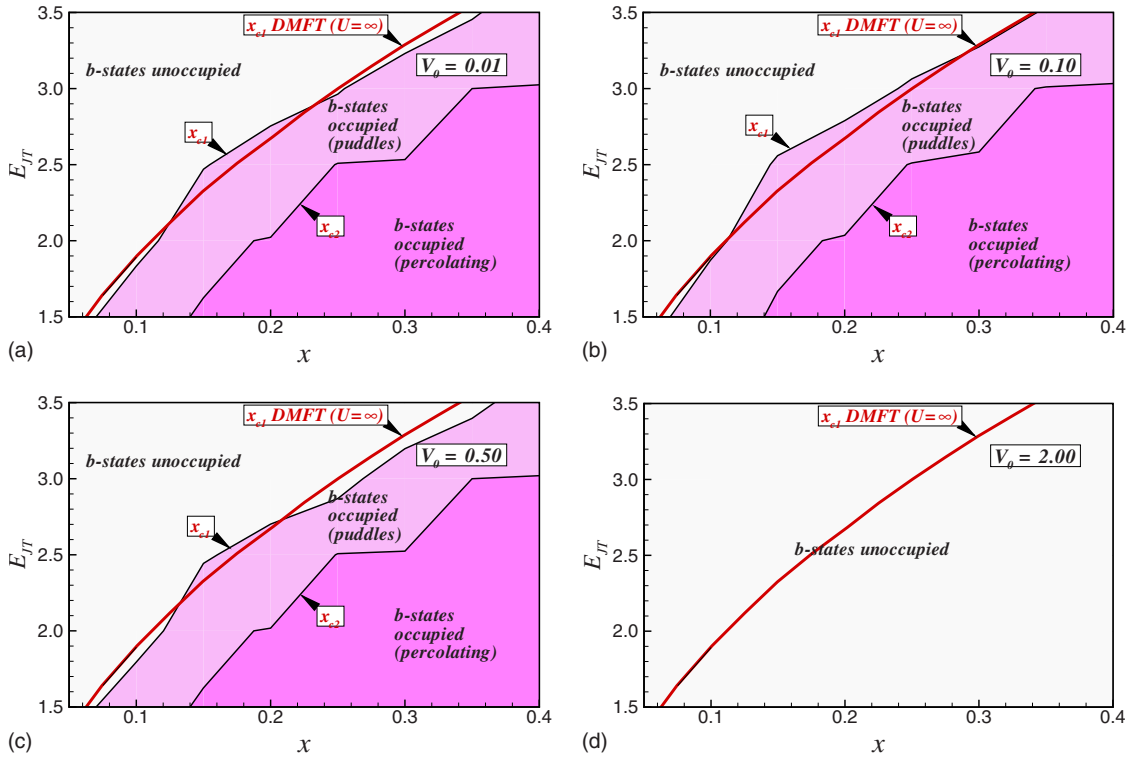

FIG. 9. (Color online) Critical doping levels x_{c1} and x_{c2} obtained from simulations. The lightest region in the contour plot contains no b electrons, the intermediate shade has "trapped" b states occupied, and the darkest regions corresponds to b states that percolate through the simulation box. The solid line corresponds to the analytical DMFT result for x_{c1}.

that the single-site DMFT, which neglects long-range Coulomb interactions and consequent nanoscale inhomogeneities or clumping and replaces it with a self consistent annealed random medium in which all sites are equivalent, is accurate for such purposes. We also note here that in the DMFT, the ℓ polaron is a single level while in the simulations the occupied levels, though localized, have a distribution of energies.

We now discuss the doping/hole density x_{c1} at which b states are occupied. In the DMFT, for $U=\infty$ and at $T=0$, the critical concentration x_c at which the lowest energy b state is occupied is $x_{c1}=(E_{JT}/D_0)^2$, where D_0 is the bare half bandwidth.[17] From our simulations, the ℓ chemical potential μ (i.e., the energy of the last occupied ℓ state) is $-E_{JT}+A(x)V_0$. At the onset of the occupation of the b states, equilibrium demands that the bottom of the b band has to just equal the chemical potential μ. Noting that the effective half bandwidth of the b band is $D_0\sqrt{x}$ and the band center $E_b=B(x)V_0$, one obtains on equating the b band bottom to the chemical potential a result for the critical doping

$$\sqrt{x_{c1}} = \frac{E_{JT}}{D_0} + [A(x_c) - B(x_c)]\frac{V_0}{D_0}. \tag{34}$$

Since $A(x)\approx B(x)\approx 1$, and $V_0/D_0 \leq 0.05$ (typically) x_{c1} is expected to be very close to the DMFT value. In Fig. 9, we notice that as expected, for small/realistic values of V_0, there is good agreement with DMFT and the simulation results. For larger values of V_0 (of the order of D_0), b state occupancy needs much larger hole density x than implied in the DMFT. Indeed, there is critical value of $V_0(V_0^c \approx 1.2)$ above which there is no band occupancy for $E_{JT}\geq 1$; the system becomes a Coulomb glass of ℓ polarons.

Furthermore, unlike in the DMFT, in the present context the fact that b states are occupied does not in itself make the system a metal. Even when $x>x_{c1}$, the hole sites where b states exist form compact clumps in our simulations. The b levels within the bigger clumps which are below the chemical potential and are occupied are hence still localized. Figure 10 shows the clumps with both the occupied and unoccupied b state regions indicated. We notice that the clumps and hence the b puddles are generally isolated. Hence the system is still an insulator. The system becomes metallic for $x>x_{c2}$ when the b *puddles* percolate, which requires as a necessary condition that the clumps with the b states occupied percolate. x_{c2} can be estimated by calculating the inverse participation ratio[38] and by checking for the geometric percolation of the clump. The differences among x_{c1} (DMFT), x_{c1} (simulations), x_{c2} (simulations), or in the nature of the b states and their occupancy are due to the fact that the single-site DMFT of the ℓb model (1) and the numerical simulation of the extended ℓb model (4) are very different approximations. In the former, the static ℓ polarons are repulsive (potential U) scattering centers for b electrons, present randomly and independently at each site with a self-consistently determined probability close to $(1-x)$. The scattering is treated in coherent potential approximation (CPA) so that there is no Anderson localization of the b electron states; there are diffusive and extended. By contrast, in the simulation, the b electrons are completely excluded from ℓ polaron sites and can hop freely from site to site only among

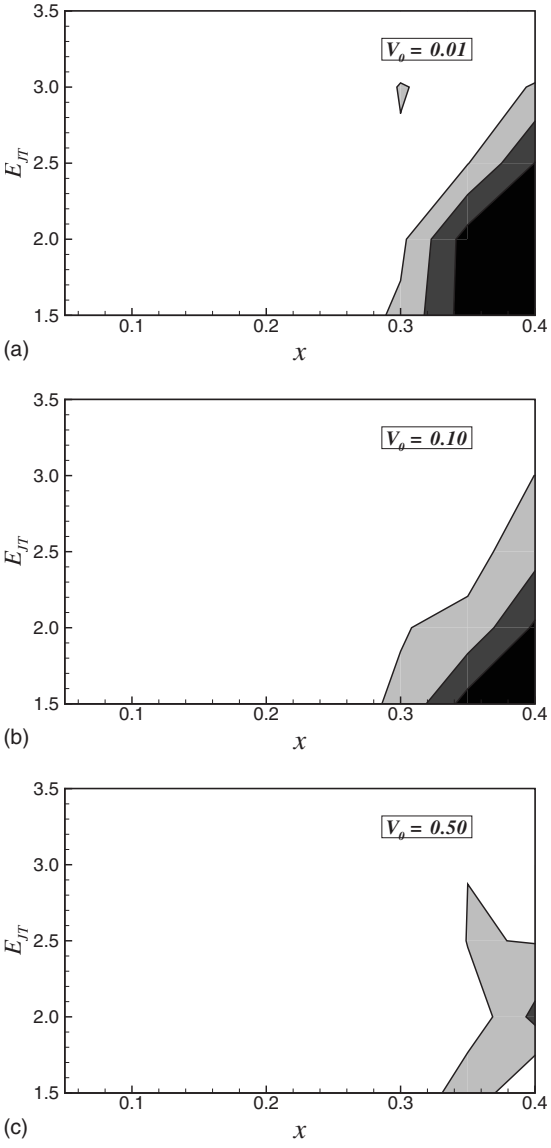

FIG. 10. Real-space structure of the electronic state. The darkest regions (magenta in online version) denote hole clumps with occupied b electrons, the lightest (white) denote hole clumps with no b electrons, the second lighter shade (cyan) denote singleton holes, and the second darkest shade (light blue) represents regions with ℓ polarons. The simulations for each V_0 are for the same realization of the random distribution of Ak ions. The cell size is $16\times16\times16$.

contiguous hole sites (clumps). So unless the clumps are connected percolatively, the system is an insulator. Furthermore, even when the clumps percolate, if the ℓ polaron distribution and the b electron propagation in such an ℓ polaron medium could be treated realistically, one will find that in contrast to single-site DMFT, a fraction of the occupied b states are Anderson localized due to the ℓ polaron disorder and the repulsion $Un_{\ell i}n_{bi}$. Hence x_{c2} is larger than the value of x at which the clumps just percolate, as the highest occupied b state could still be Anderson localized within the percolating clump; hence x_{c2} signifies the value of x at which the *mobility edge* in the b band crosses the chemical potential.

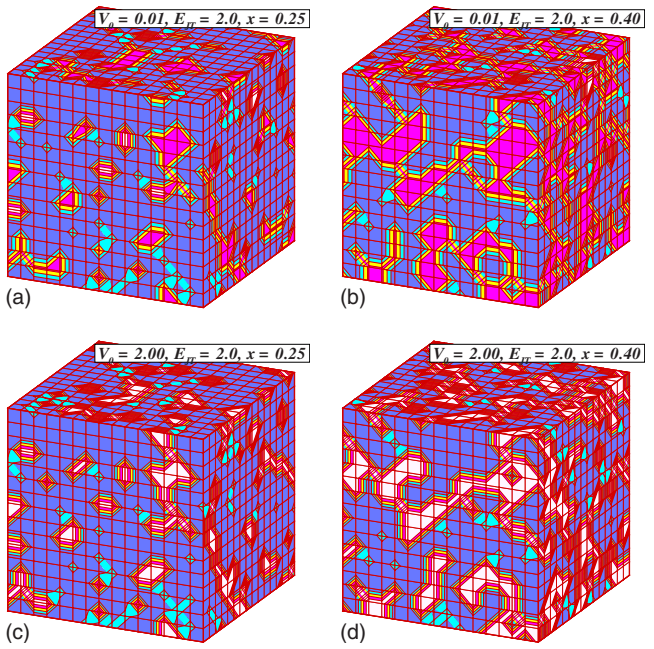

FIG. 11. (Color online) Dc conductivity $\sigma(\omega\approx0)$ as a function of system parameters. For long long-range Coulomb parameter V_0 greater than 0.4, the conductivity is zero for the indicated range of E_{JT} and x. The darkest shade of the contour corresponds to a dimensionless conductivity $\sigma>10$, the next darkest $5>\sigma\geq10$, the lightest $0>\sigma>5$.

We have confirmed this by calculating the contribution of the b states to the dc conductivity using the standard Kubo formalism[39]—the results, in the form of contours of constant dc conductivity in the E_{JT}, x plane, are shown in Fig. 11. Again, it is clear that the metal-insulator boundary (the x_{c2}) curve is independent of the long-range Coulomb parameter V_0 when V_0 is small. However, the dc conductivity completely vanishes for larger values of V_0 greater than V_0^m of about 0.6 and the system is an insulator (due to both strong local disorder potential from the Ak ions and Coulomb repulsion). Not unexpectedly, this critical value V_0^m is much smaller than the value V_0^c that forbids b state occupancy.

Finally, we discuss the clump size distribution. The size of a clump is defined in terms of a radius of gyration R calculated as $R=\sqrt{\{\frac{1}{n}\Sigma_{i=1}^{n}[\boldsymbol{r}(i)-\bar{\boldsymbol{r}}]^2\}}$, where $\bar{\boldsymbol{r}}$ is the center of mass of the clump and i runs over all the holes in the clump. We investigate the distribution of the quantity $(1/R)$ as a function of the system parameters for clumps with b states occupied. For a percolating clump the quantity $1/R\rightarrow0$ and for the smallest clump with two holes $1/R=2.0$. Figures 12–14 show the concentration (number per lattice site) of the *occupied clumps* as a function of their inverse size. For a given doping x and E_{JT}, there are many more larger clumps for smaller V_0 (Fig. 12). At high enough V_0 ($V_0=2.0$) there are no b electron puddles. The effect of doping x is also as expected. At small doping, there are clumps of various sizes, while at larger doping, there is only one percolating clump (see Fig. 13). The effect of E_{JT} is more interesting (Fig. 14). For $E_{JT}=1.50$ there is a percolating clump together with isolated small puddles. On increase in E_{JT} ($E_{JT}=2.0$), the isolated electron puddles are larger in size and on further in-

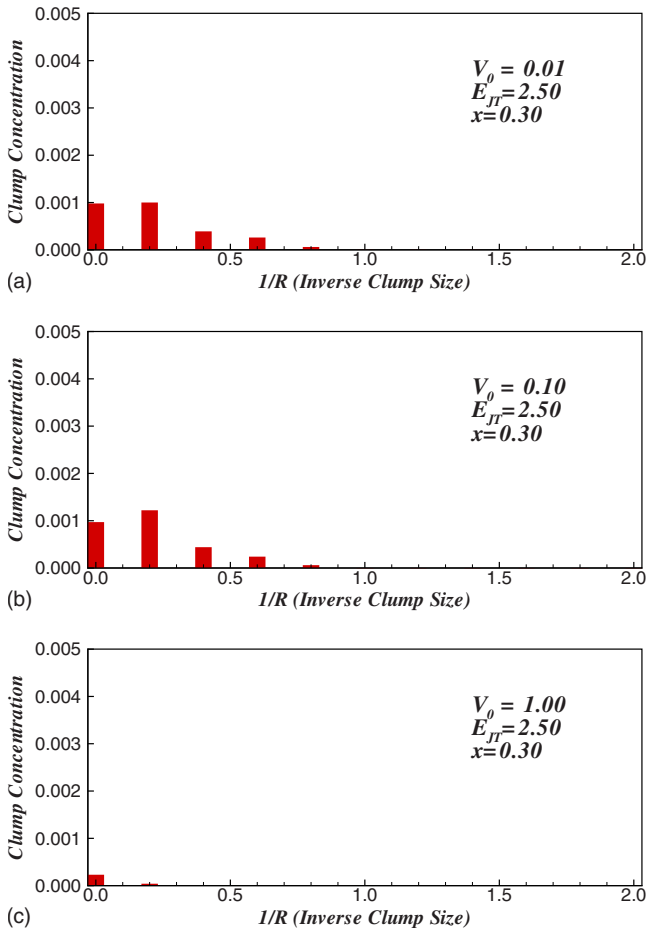

FIG. 12. (Color online) Size distribution of clumps with occupied b electrons. Clump concentration is number of clumps per lattice site (simulated with a $10\times10\times10$ box). Size of the clump R is the "radius of gyration" of the clump (see text), ordinate is inverse clump size. $1/R=0$ corresponds to a percolating clump, while $1/R=2$ corresponds to the smallest clump with two sites. The plots show the effect of the Coulomb interaction V_0 on the distribution for $x=0.3$ and $E_{JT}=2.5$. For $V_0=2.00$ there are no clumps with occupied b electrons.

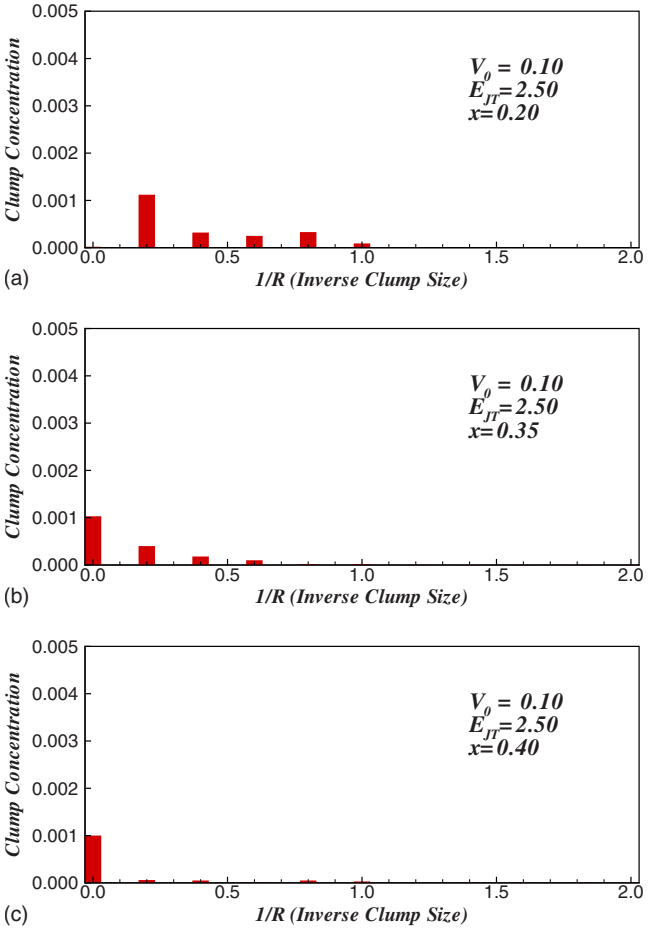

FIG. 13. (Color online) Size distribution of clumps with occupied b electrons. Clump concentration is number of clumps per lattice site (simulated with a $10\times10\times10$ box). Size of the clump R is the radius of gyration of the clump (see text), ordinate is inverse clump size. $1/R=0$ corresponds to a percolating clump, while $1/R=2$ corresponds to the smallest clump with two sites. The plots show the effect of the doping x on the distribution for $V_0=0.1$ and $E_{JT}=1.0$. For $x\geq0.4$ there is only one percolating clump.

crease in E_{JT} ($E_{JT}=3.0$), there is essentially a single large percolating puddle. This is due to the fact that occupancy of a clump requires that the gain in kinetic-energy offsets the loss in the Jahn-Teller energy E_{JT} at the least, thus larger E_{JT} requires larger clumps to be occupied for sufficient gain in kinetic energy. Figure 15 shows the dependence of the average inverse size $(1/R^{oc})_{av}$ on the parameters; the results are as expected, in that the average size of clumps is about a few lattice spacings for small doping ($x<0.25$), followed by a regime of percolating clumps. A result of particular interest is the dependence of the average clump size on the long-range Coulomb parameter V_0. This result is plotted in Fig. 16; we see that the clump size is essentially insensitive to V_0 until V_0 approaches t. This may be contrasted with the simple analytical result obtained earlier (see Fig. 3). It is evident that the real system, any finite V_0 will prevent phase separation, but the final details of the ground state is strongly determined by the *random* distribution of the Ak ions, which also determines the size scale of the clumps (and hence their insensitivity to V_0 for small values of V_0). We have investigated the size dependence of the clump size on the size of the simulation cube and found that there is no significant size dependence.

Our study therefore indicates that for small doping ($x<0.25$), electronic inhomogeneities in the form of localized b electron puddles exist in a background of polarons (see Fig. 10) while for larger doping, the system consists of intermingled states of percolating delocalized b electron puddles coexisting with regions of localized ℓ polarons. The scale of the inhomogeneities is that of the local Ak ion disorder and not much larger. The study therefore confirms that long-range electrostatic interactions gives rise to only nanometer (or lattice scale) electronic inhomogeneities as was anticipated in earlier literature.[9] The key point is that this nanometric scale arises not out of phase competition but due to strong correlation effects of two types of states that appear at the atomic scale, whose spatial arrangement is then controlled by the long-range Coulomb interaction and the random distribution of the Ak ion disorder.

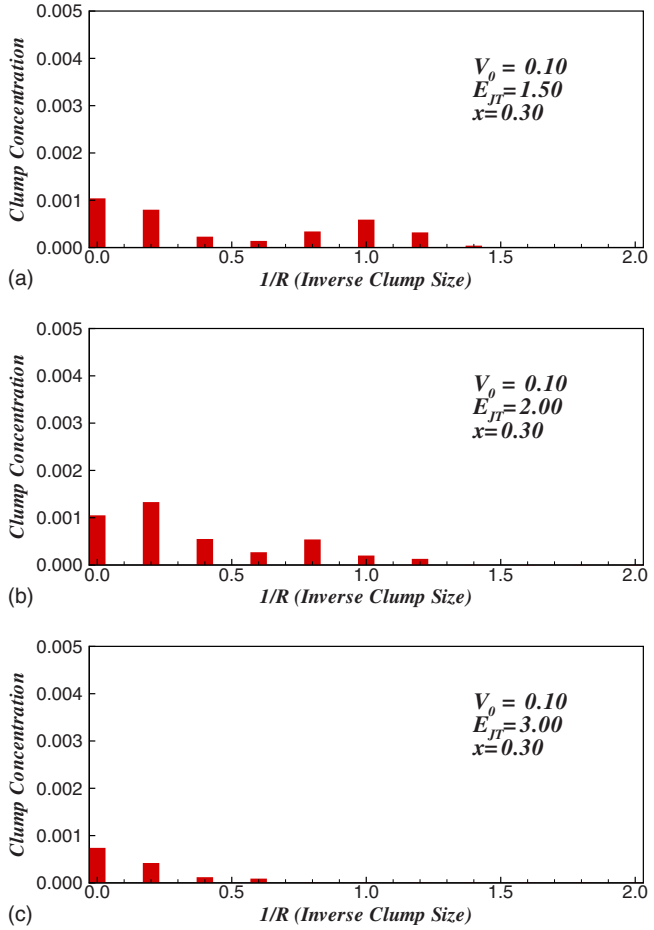

FIG. 14. (Color online) Size distribution of clumps with occupied b electrons. Clump concentration is number of clumps per lattice site (simulated with a $10\times10\times10$ box). Size of the clump R is the radius of gyration of the clump (see text), ordinate is inverse clump size. $1/R=0$ corresponds to a percolating clump, while $1/R=2$ corresponds to the smallest clump with two sites. The plots show the effect of E_{JT} on the distribution for $V_0=0.1$ and $x=0.3$. For $E_{JT}=3.5$ there are no occupied clumps.

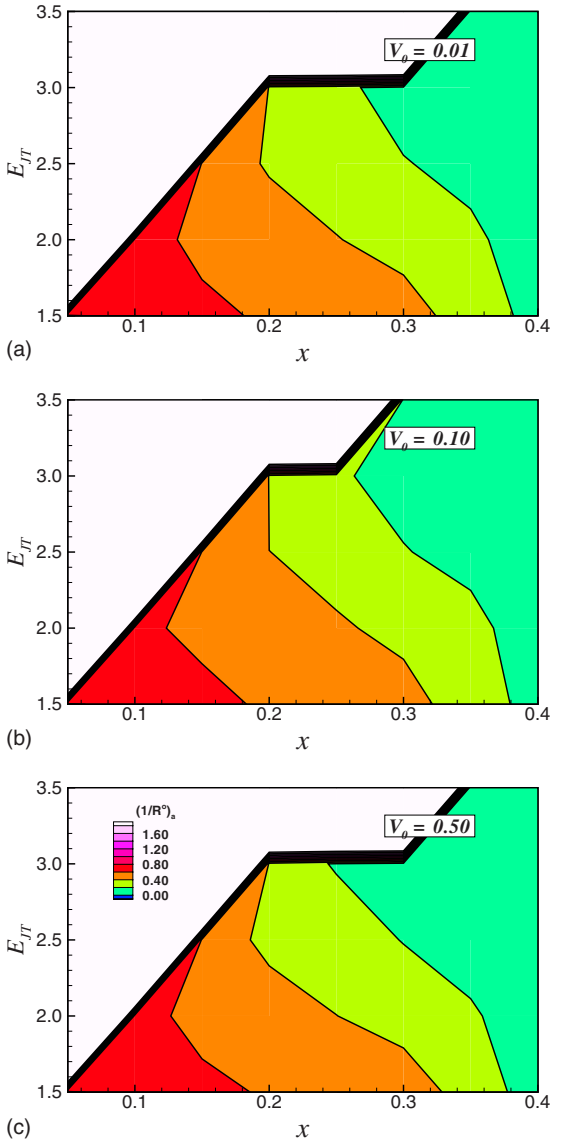

FIG. 15. (Color online) Average inverse size $(1/R^o)_a$ of the clumps with at least one b state occupancy. Clump size R is defined as the radius of gyration (see text) of the clump. For small V_0, the average inverse size at $x=0.2$ and $E_{JT}=1.0$ is between 0.44 and 0.88—thus corresponds to spherical puddle of containing 6–10 lattice sites. With increase in V_0, the sizes decreases and eventually there are no occupied clumps at $V_0=2.0$ (not shown). At larger x, there is one percolating clump for $V_0\lesssim1.0$. At larger E_{JT}, again, there are no occupied clumps.

IV. DISCUSSION

Our study of the extended ℓb model has established that long-ranged Coulomb interaction gives rise to nanoscale electronic inhomogeneities. A key point is that even a very small V_0 completely eliminates the macroscopic phase-separation tendency of the Falicov-Kimball-like ℓb model (compare Fig. 1 with Fig. 10). By using a dielectric constant of about 20, we estimate an upper bound for V_0 in manganites to be about 0.02 eV and thus well within the small V_0 regime; for $t\approx0.2$ eV, the dimensionless V_0 is about 0.1. Furthermore, for a given set of energy parameters (V_0 and E_{JT}), we have shown the existence of two important doping thresholds: x_{c1} which corresponding to the occupancy of the b states, and $x_{c2}>x_{c1}$ at which there is an insulator to metal transition. Our results for x_{c1} are close those of the earlier DMFT prediction; however, the present work predicts the existence of x_{c2}, a feature that is absent in DMFT (in DMFT $x_{c2}=x_{c1}$). The key physics behind the agreement of x_{c1} is *the large U* condition (no simultaneous occupancy of ℓ polaron and b electron on one site), and the random distribution of the Ak ions. As we have shown, the random distribution of Ak ions produces local clustering of holes around them which eventually causes electron puddles and subsequent percolating clumps at higher doping. The main consequence is that the electronic inhomogeneities are all at the nanoscale and the material appears homogeneous at microscale.

How important is the random distribution of Ak ions? This question was answered by distributing the charge of the Ak ions equally among all the Ak sites. The physics of the problem is changed completely by this step. First, the clustering tendency of the holes is completely suppressed. This is

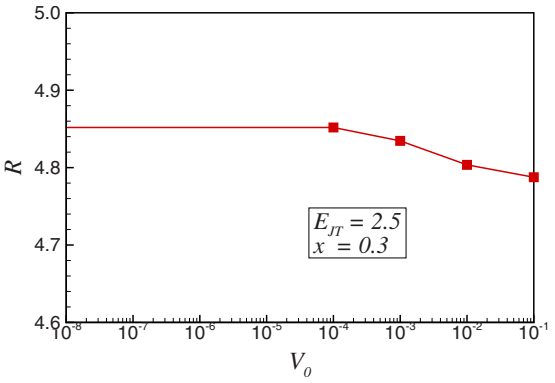

FIG. 16. (Color online) Clump size as a function of the Coulomb interaction parameter V_0 (normalized by t) for $E_{JT}=2.5t$, $x=0.3$ obtained from simulations.

evident from Fig. 7 (right column) where it is seen that the probability of finding a hole neighboring a hole is nearly reduced to zero. In such a case, for a given set of energetic parameters, much larger doping levels would be required for b state occupancy, and for the insulator to metal transition. Indeed, these observations are borne out in the full scale simulations, see Fig. 17. Thus the physically more realistic random distribution of Ak ions is key to the agreement with the DMFT calculation. In other words, the earlier DMFT calculation, although it did not take into account the long-range Coulomb interactions, premised a homogeneous state (on a "macroscopic" scale), thereby effectively incorporating the key effect of the long-ranged Coulomb interaction.

It may be argued that effects of the random distribution of Ak ions (that help the clustering of holes) is equivalent to a local disorder potential. The results of the ℓb Hamiltonian (1) with an additional disorder potential (but no long-range Coulomb interactions),

$$\mathcal{H}_{dis} = \sum_i w_i \ell_i^\dagger \ell + \sum_j w_j b_j^\dagger b_j, \tag{35}$$

where w_j are distributed uniformly between $-W$ and W, should be roughly similar to those of the extended ℓb Hamiltonian (1). The premise is that since ℓ electrons will occupy sites of low w_i, holes are likely to clump with a probability proportional to x^n where n is the size of the clump. This is similar to the probability of finding clustering together of Ak ions. Thus the clumps that appear in the disorder only model may be expected to have similar nature as that of the case with random distribution of Ak ions. The results of the disorder-only Hamiltonian are shown in Fig. 18. Clearly, the result of x_{c1} is close to that of the DMFT and the extended ℓb results. Also, the clump sizes, etc. are also quite similar as expected. There is, however, a crucial difference—the density of states of the ℓ electrons does not have a Coulomb-type gap in the purely disordered model just discussed. In the real system both disorder and long-ranged Coulomb interactions are present, and the extended ℓ-b model includes both in a realistic way, in contrast to the disorder only model.

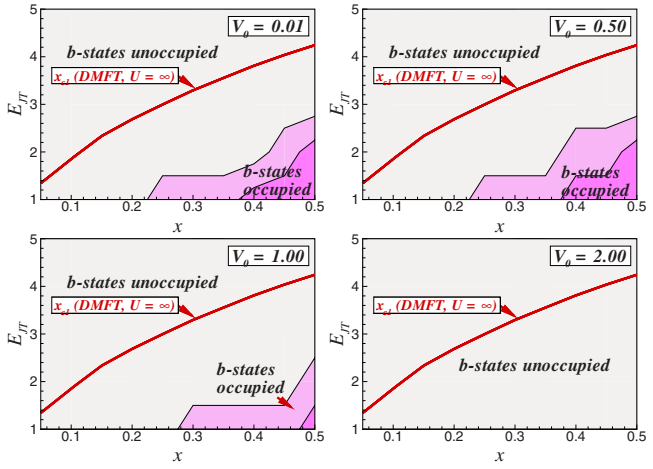

FIG. 17. (Color online) Critical doping levels x_{c1} and x_{c2} obtained from simulations with uniform distribution of Ak ions. The contour scheme is same as that of Fig. 9. These results are for one initial realization of the holes (no average over initial conditions).

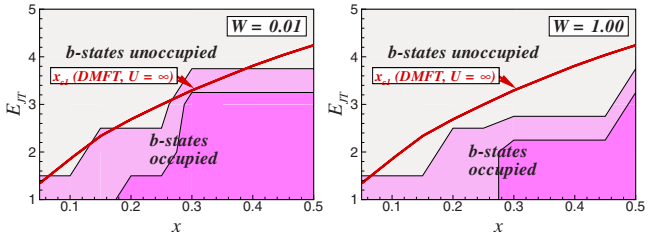

FIG. 18. (Color online) Critical doping levels x_{c1} and x_{c2} obtained from simulations with on-site disorder which varies from $-W$ to $+W$. The contour scheme is same as that of Fig. 9. These results are for one realization of the disorder.

We now discuss further predictions and inferences from the model. Our model is particularly suited to study the low bandwidth manganites such as Pr based compounds which have a large ferroinsulating regime as a function of doping. Most of the inferences made hinge on the coexistence of localized and delocalized states—the key physical idea of the ℓb model. It may be inferred from the extended ℓb model that the low-temperature conductivity in the low-temperature regime for doping $x<x_{c1}$ will be governed by the polaron Coulomb glass. Thus, the low-temperature conductivity is expected to be that predicted by for the Coulomb glass,[23] i.e., $\sigma(T) \sim e^{-a/\sqrt{T}}$, where a is a constant. Further, above $x_{c2}>x>x_{c1}$, several excitations contribute to the conductivity. These will include polaron hopping, variable range hopping of the b-state electrons from one puddle to the other, even two step processes where a b-state in an intermediate for an ℓ-polaron to hop from one site to another. Transport in this regime is therefore expected to be involved and further investigation is necessary to uncover the temperature dependence. We note that transport measurements[40] on doped manganites do show the features that we deduce from our model. For $x>x_{c2}$, the low-temperature conductivity will be metallic with large residual resistivity. An important contribution to this resistivity arises from the Coulomb potentials of the Ak ions as has been noted earlier.[41] At higher temperatures, scattering from the thermally disordered t_{2g} spins will cause a decrease in the effective bandwidth of the b states and can lead to the opening up of a gap between the ℓ states and the b states above the ferromagnetic transition temperature. In this high-temperature regime the conductivity will have con-

tributions both from polaron hopping and thermal excitations of the ℓ polarons to the b states similar to that of a semiconductor.

The present model does not explicitly include the t_{2g} core spins as degrees of freedom. A simple minded approach of including these degrees of freedom will lead to intractable computational complexities. Novel approaches to treat both Coulomb interactions, b state quantum effects, and core spins need to be developed to attain a final understanding of the manganite puzzle.

We conclude the paper with a discussion of the important issue of phase separation and electronic inhomogeneities. As noted in the introductory section several groups have implied that the presence of electronic inhomogeneities is *essential* for the occurrence of the colossal magnetoresistance. Our work suggests that inhomogeneities are only present at the nanometer scale and a theory that *averages over these* without explicit treatment of these inhomogeneities can and does reproduce colossal magnetoresistance.[17–19] Indeed, very recent experimental work[16] shows that materials with no detectable phase separation show colossal magnetoresistance. Further, we find that nanoscale inhomogeneities are a direct result of long-range Coulomb interaction frustrating phase separation induced by *strong correlation*—nanoscale electronic inhomogeneities are not a result of phase competition in our model. Although similar mechanisms based on long-range coulomb interactions has been discussed earlier,[9,42–45] we believe that this is the first detailed quantitative treatment of a realistic model any correlated oxide.

The large length scale (micrometer sized) inhomogeneities seen in experiments remain to be explained in the present framework. To the best of our knowledge, the coexistence of metallic and insulating regions have all been seen only in surface probe measurements or measurements with thin films (for electron microscopy). Creation of a surface introduces defects such as cracks and steps all of which have long-ranged elastic fields. As is well known, the phase of manganites is strongly influenced by pressure (stresses).[46] Thus the large scale inhomogeneities are likely to be a result of pre-existing strain sources as is indicated by recent photoemission experiments.[7] It is possible to explicitly test this in an experiment (see Fig. 19) with a precracked manganite sample—on loading the cracked sample the motion of the metal-insulator boundary is expected to be observed. Similar experiments[47] (without cracks, etc.) do indeed suggest the strong effects of strains.

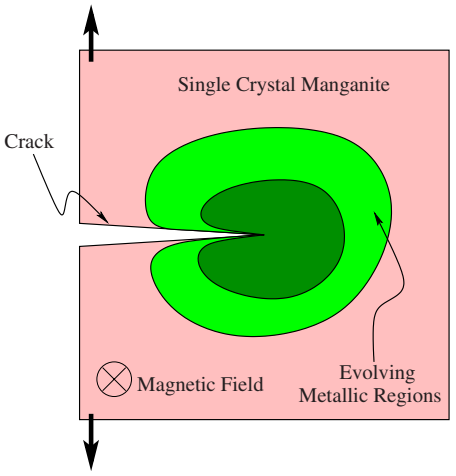

FIG. 19. (Color online) Schematic of a suggested experiment to study the influence of long-range strain effects on mesoscale inhomogeneities in manganites.

A second possibility for the existence of micronscale clusters could be due to "kinetic arrest" as seen recently in some rare-earth compounds.[48] Thus the patches that appear could arise to an "incomplete phase transition" and likely to show "glassy" behavior. Indeed many manganites are known to show glassy behavior,[2] and this is possibly another important line of further investigation.

ACKNOWLEDGMENTS

V.B.S. wishes to acknowledge generous support from the DST, India, through a Ramanujan grant. H.R.K. acknowledges support from the Department of Science and Technology, India through a J. C. Bose grant. T.V.R. acknowledges support from DST via the Ramanna grant, and NCBS, Bangalore for hospitality. We thank Pinaki Majumdar, D. D. Sarma, Dinesh Topwal, and A. K. Raychaudhuri for useful discussions. A special note of thanks to P. Sanyal for discussions and data analysis.

*shenoy@physics.iisc.ernet.in
†gupta@physics.iisc.ernet.in
‡hrkrish@physics.iisc.ernet.in
§tvrama@bhu.ac.in

[1] E. Dagotto, Science **309**, 257 (2005).
[2] E. Dagotto, New J. Phys. **7**, 67 (2005).
[3] M. Uehara, S. Mori, C. H. Chen, and S. W. Cheong, Nature (London) **399**, 560 (1999).
[4] C. Renner, G. Aeppli, B. G. Kim, Y.-A. Soh, and S.-W. Cheong, Nature (London) **416**, 518 (2002).
[5] M. Fäth, S. Freisem, A. A. Menovsky, Y. Tomioka, J. Aarts, and J. A. Mydosh, Science **285**, 1540 (1999).
[6] L. Zhang, C. Israel, A. Biswas, R. L. Greene, and A. de Lozanne, Science **298**, 805 (2002).
[7] D. D. Sarma, D. Topwal, U. Manju, S. R. Krishnakumar, M. Bertolo, S. La Rosa, G. Cautero, T. Y. Koo, P. A. Sharma, S.-W. Cheong, and A. Fujimori, Phys. Rev. Lett. **93**, 097202 (2004).
[8] E. Dagotto, T. Hotta, and A. Moreo, Phys. Rep. **344**, 1 (2001).
[9] E. Dagotto, *Nanoscale Phase Separation and Colossal Magnetoresistance* (Springer-Verlag, Berlin, 2003).
[10] C. N. R. Rao, A. K. Kundu, M. M. Seikh, and L. Sudheendra, Dalton Trans. 2004, 3003.
[11] V. B. Shenoy, D. D. Sarma, and C. N. R. Rao, ChemPhysChem **7**, 2053 (2006).

[12] P. Lee, N. Nagaosa, and X.-G. Wen, Rev. Mod. Phys. **78**, 17 (2006).
[13] J. Burgy, M. Mayr, V. Martin-Mayor, A. Moreo, and E. Dagotto, Phys. Rev. Lett. **87**, 277202 (2001).
[14] E. Dagotto, J. Burgy, and A. Moreo, Solid State Commun. **126**, 9 (2003).
[15] C. Sen, G. Alvarez, and E. Dagotto, Phys. Rev. Lett. **98**, 127202 (2007).
[16] R. Mathieu, D. Akahoshi, A. Asamitsu, Y. Tomioka, and Y. Tokura, Phys. Rev. Lett. **93**, 227202 (2004).
[17] G. V. Pai, S. R. Hassan, H. R. Krishnamurthy, and T. V. Ramakrishnan, Europhys. Lett. **64**, 696 (2003).
[18] T. V. Ramakrishnan, H. R. Krishnamurthy, S. R. Hassan, and G. V. Pai, *Colossal Magnetoresistive Manganites*, edited by T. Chatterji (Kluwer, Dordrecht, 2003).
[19] T. V. Ramakrishnan, H. R. Krishnamurthy, S. R. Hassan, and G. Venketeswara Pai, Phys. Rev. Lett. **92**, 157203 (2004).
[20] Y. Imry and S.-K. Ma, Phys. Rev. Lett. **35**, 1399 (1975).
[21] K. H. Ahn, T. Lookman, and A. R. Bishop, Nature (London) **428**, 401 (2004).
[22] H. R. Krishnamurthy, Pramana **64**, 1063 (2005); Invited talk published in the Proceedings of the 22nd IUPAP International Conference on Statistical Physics, edited by S. Dattagupta, H. R. Krishnmurthy, R. Pandit, T. V. Ramakrishanan, and D. Sen.
[23] A. L. Efros and B. I. Shklovskii, J. Phys. C **8**, L49 (1975).
[24] V. B. Shenoy, T. Gupta, H. R. Krishnamurthy, and T. V. Ramakrishnan, Phys. Rev. Lett. **98**, 097201 (2007).
[25] N. Furukawa, J. Phys. Soc. Jpn. **64**, 2754 (1995).
[26] A. J. Millis, R. Mueller, and B. I. Shraiman, Phys. Rev. B **54**, 5405 (1996).
[27] J. K. Freericks and V. Zlatić, Rev. Mod. Phys. **75**, 1333 (2003).
[28] A. Georges, G. Kotliar, W. Krauth, and M. J. Rozenberg, Rev. Mod. Phys. **68**, 13 (1996).
[29] O. Cepas, H. R. Krishnamurthy, and T. V. Ramakrishnan, Phys. Rev. Lett. **94**, 247207 (2005).
[30] O. Cepas, H. R. Krishnamurthy, and T. V. Ramakrishnana, Phys. Rev. B **73**, 035218 (2006).
[31] J. K. Freericks, E. H. Lieb, and D. Ueltschi, Phys. Rev. Lett. **88**, 106401 (2002).
[32] K. I. Kugel, A. L. Rakhmanov, and A. O. Sboychakov, Phys. Rev. Lett. **95**, 267210 (2005).
[33] A. L. Efros, J. Phys. C **9**, 2021 (1976).
[34] T. Vojta and M. Schreiber, Philos. Mag. B **81**, 1117 (2001).
[35] S. D. Baranovskii, A. L. Efros, B. L. Gelmont, and B. I. Shklovskii, J. Phys. C **12**, 1023 (1979).
[36] J. H. Davies, P. A. Lee, and T. M. Rice, Phys. Rev. B **29**, 4260 (1984).
[37] C. Kittel, *Introduction to Solid State Physics*, 7th ed. (Wiley & Sons, New York, 1996).
[38] D. J. Thouless, Phys. Rep. **13**, 93 (1974).
[39] G. D. Mahan, *Many-particle Physics* (Kluwer Academic/Plenum Publishers, Dordrecht/New York, 2000).
[40] L. Sudheendra and C. N. R. Rao, J. Phys.: Condens. Matter **15**, 3029 (2003).
[41] W. E. Pickett and D. J. Singh, Phys. Rev. B **55**, R8642 (1997).
[42] E. Nagaev, *Physics of Magnetic Semiconductors* (MIR, Moscow, 1983).
[43] V. J. Emery, S. A. Kivelson, and H. Q. Lin, Phys. Rev. Lett. **64**, 475 (1990).
[44] V. J. Emery and S. A. Kivelson, Physica C **209**, 597 (1993).
[45] J. Lorenzana, C. Castellani, and C. Di Castro, Phys. Rev. B **64**, 235127 (2001).
[46] P. Postorino, A. Congeduti, P. Dore, A. Sacchetti, F. Gorelli, L. Ulivi, A. Kumar, and D. D. Sarma, Phys. Rev. Lett. **91**, 175501 (2003).
[47] M. Paranjape, A. K. Raychaudhuri, N. D. Mathur, and M. G. Blamire, Phys. Rev. B **67**, 214415 (2003).
[48] M. K. Chattopadhyay, S. B. Roy, and P. Chaddah, Phys. Rev. B **72**, 180401(R) (2005).